73.2

S193 RADIOMETER BRIGHTNESS
TEMPERATURE PRECISION/ACCURACY
FOR SL2 AND SL3
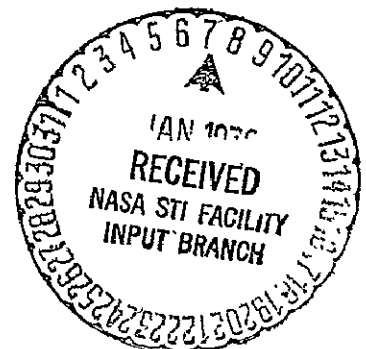# (SPE-S193-012, S&AD)

Job Order 75-215

Prepared By

Lockheed Electronics Company, Inc.
Aerospace Systems Division
Houston, Texas

Contract NAS 9-12200

For

EARTH OBSERVATIONS DIVISION

National Aeronautics and Space Administration
LYNDON B. JOHNSON SPACE CENTER
Houston, Texas

June 1975

LEC-5976

JSC-09793

S-193 RADIOMETER BRIGHTNESS TEMPERATURE
PRECISION/ACCURACY FOR SL2 AND SL3

(SPE—S193—012, S&AD)

Job Order 75-215

PREPARED BY

(signature)

D. J. Pounds, Principal Engineer
Earth Observations Exploratory
Studies Department

(signature)

K. Krishen, Staff Scientist
Earth Observations Exploratory
Studies Department

APPROVED BY

(signature)

O. N. Brandt, Acting Manager
Earth Observations Exploratory
Studies Department

(signature)

J. J. Carney, Supervisor
Exploratory Investigations
Section

Prepared By

Lockheed Electronics Company, Inc.

For

Earth Observations Division

NATIONAL AERONAUTICS AND SPACE ADMINISTRATION
LYNDON B. JOHNSON SPACE CENTER
HOUSTON, TEXAS

June 1975

LEC-5976

ii

ABSTRACT

The NASA Skylab Sensor Performance Evaluation task SPE-S193-012 is concerned with estimating the precision and accuracy with which the S193 Radiometer measured the brightness temperature of ground scenes. These estimates were derived from data collected during Skylab missions. For this study, homogeneous ground sites were selected and S193 Radiometer Brightness Temperature data analyzed. The precision was expressed as the standard deviation of the radiometer acquired brightness temperature. Precision was determined to be 2.40 K or better depending on mode and target temperature.

The indication of the measurement accuracy was derived from various comparisons. A theoretical scattering formula most suitable to the surface model was selected. Ground parameters were used to evaluate the theoretical values of brightness temperatures of homogeneous smooth water sites. Through this procedure, the lower limiting set of brightness temperatures was generated for certain sites. As a final step, the differences between the actual measured values and those developed using mathematical models were computed. These differences were indicative of the accuracy of measurement. This analysis indicates that bias errors probably did not exceed 3° K for hot targets, 8° K for water targets, and 14° K for deep space. Some modes gave better results.

ACKNOWLEDGMENTS

CONTENTS

viii

TABLES

FIGURES

S193 RADIOMETER BRIGHTNESS
TEMPERATURE PRECISION/ACCURACY
FOR SL2 AND SL3
(SPE-S193-012, S&AD)

1.0   INTRODUCTION

Scientific measurements by the S193 Radiometer will be
more valuable if accurate estimates of errors in the final
measured value are available. The prime errors of concern
are in precision and accuracy. Since there are disagree-
ments in the literature concerning definitions of precision
and accuracy, a description of their usage is included in
this document.

Precision is a term that implies data repetition from
sample to sample over a particular target with no regard
to the bias between true and measured values of radiometric
brightness temperatures. Thus, precision is significant
to investigators who are interested in <u>differences</u> in
radiometric brightness temperatures for ground scenes of
interest as functions of the incidence angle and polarization.

Accuracy implies a measure of the bias errors plus the
statistical variations in measurement values from sample
to sample. Estimates of accuracy are important in investi-
gations which utilize <u>absolute values</u> of radiometric bright-
ness temperatures for correlations with phenomena of
interest.

In a classical determination of precision/accuracy,
output data from a sensor undergoing testing would be

compared with a known standard and/or an error analysis
would be performed to place upper bounds on the sensor
error.   Accurate standard instruments were not available
for comparison with the S193 Radiometer in space.   The
original S193 lab test data were not always adequate for
placing the necessary tight bounds on sensor parameters
required for a classical analysis. Therefore, estimates
of precision/accuracy are based upon a comparison of actual
S193 acquired data with measurements of brightness tempera-
tures (obtained by S194 and aircraft) and the temperatures
obtained by simulation of the target scene.

The elements involved in a complete precision/accuracy
determination are outlined in figure 1.   Most of the
important elements have been utilized in preparing this
report.   Time constraints have limited the scope of this
report.

It should be noted that any careful determination of
accuracy will be pessimistic because it will not be possible
to safely specify a least upper bound to sensor error even
if a standard instrument for comparison were available.
This problem is compounded by the fact that data from
the various sensors and references considered are gathered
from various vantage points, e.g., on the ground, from
aircraft, and from spacecraft.   For useful comparisons,
this data must be corrected to a common vantage point by
adjusting for the effects of the atmosphere.   This is
illustrated in figure 1.   The common point chosen for
comparison in this study was the S193 vantage point.

Figure 1. – Elements in precision/accuracy determination.

1-3

Since no standard instrument is available, the output from S193 production data processing will be compared with data derived from parallel experimental and/or analytical paths. This is also shown in figure 1.

Reference information, ephemerides, and ground scene characteristics, viewed by each sensor used, enter into the selection of common ground data scenes. The ground data cells are viewed by each sensor from their own vantage points. This data enables the selection of a valid data subset which is applicable to a common scene. This data subset must be adjusted to account for the effects of atmosphere above the sensor by utilizing the results of the atmospheric models where necessary. Data from each of the sensors is then statistically analyzed to produce the calculated radiometric temperatures and their uncertainties for selected ground scenes.

Modeling plays a key role in the precision/accuracy process. Reference information on the ground scene, data gathered from ground sensors, and data gathered from airborne and spaceborne sensors (except S193), which have been corrected to ground level using atmospheric models, are combined into ground scene models. Flight/field-of-view models, atmospheric models, and S193 antenna models determine what portion of the ground scene are viewed. The ground scene models are atmospherically corrected to Skylab level for final comparisons.

The atmospheric model is based upon reference information concerning properties of the atmosphere.

The function which models the S193 antenna is based
upon test data but uses a symmetrical antenna pattern. The
data output from the S193 antenna model is passed through a
computer simulation of the S193 radiometer.[1] Resulting
simulated data are processed using a copy of the production
data processing algorithm. These processed simulation data
are used for comparison with S193 and other sensor data,
for initiation of any necessary corrections in the models,
and for production data processing.

The parallel data paths resulting from simulation
models, S193 itself, EREP, ground, and airborne sensors are
described in more detail in sections 2.0 through 6.0. In
section 7.0, the results for the parallel paths are compiled
and compared mission-by-mission and site-by-site.

Conclusions regarding precision are developed in
section 8.0 and conclusions on accuracy are compiled in
section 9.0. Section 10.0 contains a summary and
recommendations.

2.0 SIMULATION MODELS

Even a casual examination of figure 1 reveals that much
data comparison depends heavily upon the simulation models.
Figure 2 illustrates the relationship between the simulation
models and the actual S193 system and its environment. It
should be noted that the simulation system makes a number
of simplifying assumptions. For example, for analytical
calculations, a 2.8° K cosmic background is assumed and
radiations from other radio-astronomy sources (such as the
sun, moon, planets, stars, and galaxy) are neglected or
assumed to be zero. Where possible, data that is known to
be significantly affected by the sun and moon are discarded.
The deep space and ground scene models are initially covered
in section 2.1. In 2.2, atmosphere models are discussed.
Sections 2.3 and 2.4 are devoted to flight path/field-of-
view and antenna models. Section 2.5 describes the radio-
meter simulation model. Finally, section 2.6 discusses the
processing of simulated data.

2.1 Target Models

In the following sections, models for deep space, smooth
ocean, rough ocean, land, and mixed scenes are discussed.
The models for smooth ocean and atmosphere presented here
are adapted from the work of Paris.[2,3,4]

The target simulation models are developed in terms of
sky temperature background, target surface emissivity, and
characteristics of any intervening media.

2-1

(a) Expected or simulated processed data parallels the actual processed data.
(b) Simulated data is processed by using a copy of production data processing.
(c) Output of the sensor model is the simulated data.
(d) S193 sensor model simulates S193 electronics.
(e) Flight path/FOV simulation model gives effects of gimbals.

(a) S193 PROCESSED DATA

(b) PRODUCTION DATA PROCESSING

(c) UNPROCESSED S193 DATA

(d) S193 ELECTRONICS

(e) GIMBALS

S193 antenna

Simulation of S193 antenna pattern

$\vec{T}_t$ — brightness temperature of ground scene just above the surface of the earth

$\vec{T}_a$ — atmospheric anabatic radiation

$\vec{T}_k$ — atmospheric katabatic radiation

$\vec{T}_c$ — cosmic background radiation and other radio-astronomy sources

$\vec{T}_e$ — land and/or sea emission

i — incident

r — reflected from the ground

a — passed through the atmosphere

$\vec{T}_{ca}$ $\vec{T}_{ea}$ $\vec{T}_{ka}$ $\vec{T}_{aa}$

$\vec{T}_b$ sensor

$\vec{T}_c$

$\vec{T}_a$

$\vec{T}_k$

The absorbing and radiating atmosphere is represented by atmospheric models

$\vec{T}_{ci}$ $\vec{T}_{ck}$ T_t $\vec{T}_{kr}$ $\vec{T}_{ki}$

$\vec{T}_c$

land and/or sea emission and reflected energy at surface are represented by the target model.

Figure 2. — Radiation sources, viewed by S193, related to the simulation system.

ORIGINAL PAGE IS OF POOR QUALITY

2-2

Theoretical techniques, references, ground truth data, aircraft-acquired data, and data from other EREP sensors are used to arrive at the expected radiometric temperatures for S193 EREP Sensor Performance Evaluation test sites.

The ground scene simulation model includes the target emission plus the reflection of atmospheric katabatic radiation (downward, i.e., toward the earth) and cosmic background radiation which is reflected from the target's surface.

Since the cosmic radiation must pass through the entire thickness of the absorbing atmosphere and the atmospheric katabatic radiation must pass through the atmosphere beneath it, the target and atmosphere models are interlocked. The polarization-dependent nature of reflecting and scattering surfaces requires the use of vector notation in the analysis. Paris[3] gives a detailed presentation of the results summarized here:

$$\vec{T}_t = \vec{T}_{cr} + \vec{T}_{kr} + \vec{T}_e \tag{1}$$

where

$\vec{T}_t$ = Stokes vector representation of the brightness temperature of the ground scene just above the ground

$\vec{T}_{cr}$ = Stokes vector representation of the component of target brightness temperature because of cosmic radiation reflected from the surface of the ground scene

2-3

$\vec{T}_e$ = Stokes vector representation of the component of target brightness temperature due to emission from the ground scene

$\vec{T}_{kr}$ = Stokes vector representation of the component of target brightness temperature because of atmospheric katabatic radiation reflected from the target surface.

For a smooth target surface:

$$\vec{T}_{cr} = [R] \, \vec{T}_{ci} \qquad (2)$$

$$\vec{T}_{kr} = [R] \, \vec{T}_{ki} \qquad (3)$$

where

$\vec{T}_{ci}$ = Stokes vector representation of the brightness temperature of the cosmic radiation incident on the target surface

$\vec{T}_{ki}$ = Stokes vector representation of the brightness temperature of the katabatic radiation incident on the target surface.

$$[R] = \begin{bmatrix} R_1 & R_2 & 0 & 0 \\ R_2 & R_1 & 0 & 0 \\ 0 & 0 & R_3 & R_4 \\ 0 & 0 & -R_4 & R_3 \end{bmatrix} \qquad (4)$$

$$R_1 = \frac{R_v R_v^* + R_h R_h^*}{2} \qquad\qquad (5)$$

$$R_2 = \frac{R_v R_v^* - R_h R_h^*}{2} \qquad\qquad (6)$$

$$R_3 = \text{Real part of } [R_v R_h^*] \qquad\qquad (7)$$

$$R_4 = \text{Imaginary part of } [R_v R_h^*] \qquad\qquad (8)$$

R_v = reflection coefficient of the target surface for a vertically polarized signal

R_h = reflection coefficient of the target surface for a horizontally polarized signal.

An * indicates the complex conjugate of a quantity.

The target temperature equation for a smooth surface is:

$$\vec{T}_t = \vec{T}_e + [R] \, (\vec{T}_{ci} + \vec{T}_{ki}) \qquad\qquad (9)$$

Specific data or equations for $\vec{T}_{ci}$, $\vec{T}_{ki}$, and $\vec{T}_e$ will be presented in the following sections.

2.1.1 Deep Space Model. At a frequency of 13.9 GHz there is a cosmic background noise temperature variously estimated at 2°K to 4°K or more.[6] The cosmic background will be assumed to be 2.80 K for the deep-space model. Slightly different values are used alternately to take maximum advantage of previously performed work. This will not introduce significant error in the final results.

2.1.2 Smooth Sea Surface Model. Recent work, summarized by Paris[2,3,4] in the measurement of microwave brightness temperatures, has shown that if the target is a

calm sea with cloud-free atmosphere, the brightness temperature of the sea may be theoretically calculated for frequencies where the dielectric constant of sea water and atmospheric properties are known. This has been done and the results are utilized to verify the S193 flight data.

Microwave radiation emitted from below the sea-air interface encounters the surface interface and is partially transmitted and reflected. The secondary effects of reflected radiation may be neglected since sea water is a good attenuator and will dissipate microwave radiation within a few centimeters of the sea surface interface. The quantity of radiation transmitted into the atmosphere will be the microwave emission of the sea and thereby will have a brightness temperature $(\bar{T}_e)$ corresponding to the particular value of microwave emission.

Microwave radiation from the surface of the sea is a function of the thermal temperature of the surface layer, the surface roughness, the electrical properties of sea water, and the angle of incidence. The electrical properties of sea water are dependent on temperature, salinity, and frequency. Paris[3] has computed the brightness temperature of sea water due to surface emission at a number of frequencies including 10.69 GHz and 15.375 GHz.

2.1.3 Rough Sea Surface Models. Theoretical models for calculating the microwave brightness temperature of a rough sea surface have been proposed by Hall[7], Stogryn[8], Wagner and Lynch[9], and other investigators who have escaped the authors attention. Hollinger[10] has also suggested an empirical model for determining brightness temperature as a

2-6

function of wind velocity. Unfortunately, these models are not in agreement.[11] In general, however, these models indicate an increase in Microwave brightness temperature as the sea roughness increases. Since the resources and time to make an intelligent choice of rough sea models were not available, the author has not made an arbitrary choice. The smooth sea surface model developed by Paris[2,3,4] has been used as a lower bound.

     2.1.4 <u>Mixed Scene Models</u>. Some of the most important ground scenes for evaluating S193's transient response viewed during the Skylab missions were targets containing both land elements and water elements of irregular geometry. The Microwave Emission Simulation, Imaging, and Handling (MESIAH)[2] program was developed to calculate the apparent brightness temperature for simulated targets at Skylab altitudes. However, uncertainties in the calculated field-of-view (i.e. location of the data cell) for data used in this SPE task have reduced the usefulness of such a program for precision/accuracy tasks. Consequently, precision/accuracy tasks will be handled without the benefit of this program. The errors in the calculated field-of-view may be alleviated in the future.

2.2 Atmospheric Models

     The atmospheric models developed by Paris (2,3,4) are used to simulate the atmospheric emission and the absorption of radiation which passes through the atmosphere in either an upward or downward direction. The following sections will discuss atmospheric anabatic (upward) radiation, atmospheric katabatic (downward) radiation, and the absorption of energy traveling downward and upward through the atmosphere.

2.2.1 Atmospheric Anabatic Radiation. The portion of the atmospheric radiation which leaves the top of the atmosphere is a function of conditions existing in the atmosphere within the field-of-view of the S193 antenna. The analytical expression for the brightness temperature corresponding to the atmospheric anabatic radiation at the top of the atmosphere is given by equation 10.

$$\vec{T}_{aa} = \int_0^\infty \alpha(z)T(z)e^{-\int_z^\infty \alpha(z')\frac{dz'}{\mu}} \frac{dz}{\mu} \qquad (10)$$

where:

$\vec{T}_{aa}$ = Stokes vector representation of the brightness temperature corresponding to the atmospheric anabatic radiation (°K).

z = Altitude above the surface (m).

$\alpha(z)$ = Volume absorption coefficient for a unit path length (absorption due to water vapor and molecular oxygen at 13.9 GHz) (m^{-1}).

$\vec{T}(z)$ = Ambient temperature of atmospheric layer at altitude z (°K). Hereafter, the atmosphere is assumed to consist of plane-parallel, horizontally homogeneous, spherically symmetric layers.

μ = Cosine of the zenith angle.

z' = Dummy variable of integration.

The expressions for the atmospheric anabatic $(\vec{T}_{aa})$ and katabatic radiation $(\vec{T}_{ka})$ are functions of the zenith angle

and the vertical distribution of the volume absorption coefficient. This, in turn, is a function of the vertical distribution of temperature, dew-point temperature, pressure, liquid-water content, and drop-size distributions of the liquid water.

2.2.2 **Atmospheric Katabatic Radiation.** The atmosphere itself is a source of radiation and a part of this radiation reaches the surface and is called katabatic (downward) radiation. At the surface, the atmospheric katabatic radiation is partially reflected and will contribute to the total package of upwelling radiation received at the S193 antenna position. The analytical expression (neglecting scattering of the atmosphere) for the brightness temperature ($\vec{T}_{ka}$), corresponding to the atmospheric katabatic radiation at a point just above the air-sea interface before reflection occurs, is given by equation 11.

$$\vec{T}_{ka} = \int_{0}^{\infty} \alpha(z) T(z) e^{-\int_{0}^{z} \alpha(z') \frac{dz'}{\mu}} \frac{dz}{\mu} \qquad (11)$$

where:

$\vec{T}_{ka}$ = Stokes vector representation of the brightness temperature corresponding to atmospheric katabatic radiation (°K).

2.2.3 **Absorption of Downward Radiation.** Cosmic radiation from outside of the atmosphere is transmitted downward through the atmosphere and is partially absorbed by

oxygen, liquid water, and water vapor. The radiation which does reach the bottom of the atmosphere is calculated as:

$$\vec{T}_{ci} = \vec{T}_c e^{-\int_0^\infty \alpha(z) \frac{dz'}{\mu}} \tag{12}$$

where

$\vec{T}_c$ = Stokes vector representation of cosmic radiation present at the top of the atmosphere ($^\circ$ Kelvin).

$\vec{T}_{ci}$ = Stokes vector representation of cosmic radiation incident on the earth's surface ($^\circ$ Kelvin).

2.2.4 <u>Absorption of Upward Radiation.</u> Emission from the ground plus atmospheric katabatic radiation and the incident cosmic radiation reflected from the surface of the target must pass upward through the atmosphere and suffer absoprtion in the process of reaching S193, Skylab, or other airborne sensors. This may be represented by the following equation:

$$\vec{T}_{b \text{ sensor}} = \vec{T}_t e^{-\int \alpha(z) \frac{dz}{\mu}} \tag{13}$$

where

$\vec{T}_{b \text{ sensor}}$ = Stokes vector representation of the brightness temperature representing ground scene which the sensor can view from altitude Z_s.

Z = Altitude of the sensor above the surface.

The integral equations (10) through (13) are valid for a non-refracting, non-scattering atmosphere over a smooth earth at any incidence angle.

To summarize results to this point, the Stokes vector field representation of brightness temperature at the sensor may be described by:

$$\vec{T} = \vec{T}_{aa} + \vec{T}_c + \vec{T}_{ca} + \vec{T}_{ea} + \vec{T}_{ka}$$

$$= \vec{T}_{aa} + \vec{T}_c + \vec{T}_{b \text{ sensor}} \tag{14}$$

where

$\vec{T}$ = Stokes vector representation of the total brightness temperature field incident on the antenna. The other vectors remain as previously defined.

All of the Stokes vector representation will be functions of direction, i.e., they will vary with antenna pitch and roll angles.

Since the basic processes involved in the atmospheric model have been described, the next sections will be devoted to details and results for clear, cloudy, and precipitating atmospheres.

2.2.5 <u>Clear Atmosphere</u>. The model developed by Paris (2,3,4) was used to represent the atmosphere. The atmosphere chosen for use was the 1962 Standard Atmosphere.

This atmosphere has been used to approximate the conditions encountered over the test sites during SL2 and SL3.

2.2.6 <u>Cloudy Atmosphere</u>. The available model from Paris[2,3,4] requires horizontally homogeneous layers and would require a knowledge of cloud height, thickness, liquid water density, and other parameters which were not available from ground truth. Consequently, no model was developed for cloudy atmospheres.

2.2.7 <u>Precipitating Atmosphere</u>. No adequate model for precipitating atmospheres, compatible with the remainder of the required model, was available at the time this report was prepared.

2.3 Flight Path/Field-Of-View Model

Initial plans for sensor performance evaluation included simulation of sensor flight path and field-of-view for the sensor in various sun modes. No flight path/field-of-view model was available in operational form when this report was prepared. This has prevented evaluation of the instrument's transient response.

2.4 Antenna Models

The antenna model used was an analytical one utilized in conjunction with Paris' atmosphere and sea models [2,3,4]. The antenna power pattern is assumed to be circularly

symmetric (i.e., independent of ϕ) about boresight and have a power gain relative to maximum gain:

$$G(\theta,\phi) = \left[\frac{\text{sine}\left(\frac{\theta}{\theta_N}\right)}{\left(\frac{\theta}{\theta_N}\right)}\right]^f \tag{15}$$

where

$G(\theta,\phi)$ = normalized power gain of the antenna at an angle (θ,ϕ).

θ_N = beamwidth from boresight to first null in radians.

θ = angle from boresight to the point at which gain is evaluated in radians.

ϕ = azimuthal angle.

f = an exponent which is adjusted to set the side-lobe levels of the first sidelobe.

For the S193 antenna model, θ_N was set to 2.5° or 0.0436 radians and f was set to 3.4.

These parameters give a half-power beamwidth of approximately 1.7° and a first sidelobe level near -22.5 dB. The pattern is circularly symmetric. The half power beam-width was chosen slightly larger than S193 to more closely approximate the overall pattern.

The analytical model is sufficiently close to the actual S193 pattern to provide accurate results. Boresight values of brightness temperature correspond closely to those for the integrated antenna pattern. This gives strong evidence that the model is adequate since it indicates that

2-13

the net effect of a finite beamwidth of the antenna is minimal.

Limited resources have not permitted use of the actual pattern data taken by General Electric.

2.5 S193 Radiometer Sensor Model

The S193 Radiometer sensor model has been given in more detail in a previous report.[1] This mathematical simulation model produces simulated data one point at a time and does not attempt to produce a simulated data stream. A simulated data stream is not necessary for this sensor performance evaluation task.

A general description of the radiometer model follows. For modeling purpose, the S193 Radiometer was broken into a series of sensor "elements"[1]. These elements are assumed to accurately represent a particular characteristic of the component such as a circulator, a switch, a coupler, or a transmission line. A component was simulated by combining one or more of the elements described in the next paragraph. The simulated components, combined, yielded the entire S193 Radiometer subsystem simulation. In this manner, a realistic functional simulation was developed. Figure 3 shows the S193 block diagram and figure 4 depicts the sensor elements of that block diagram.

The basic elements of the S193 Radiometer simulated model are the following:

● Dissipative loss
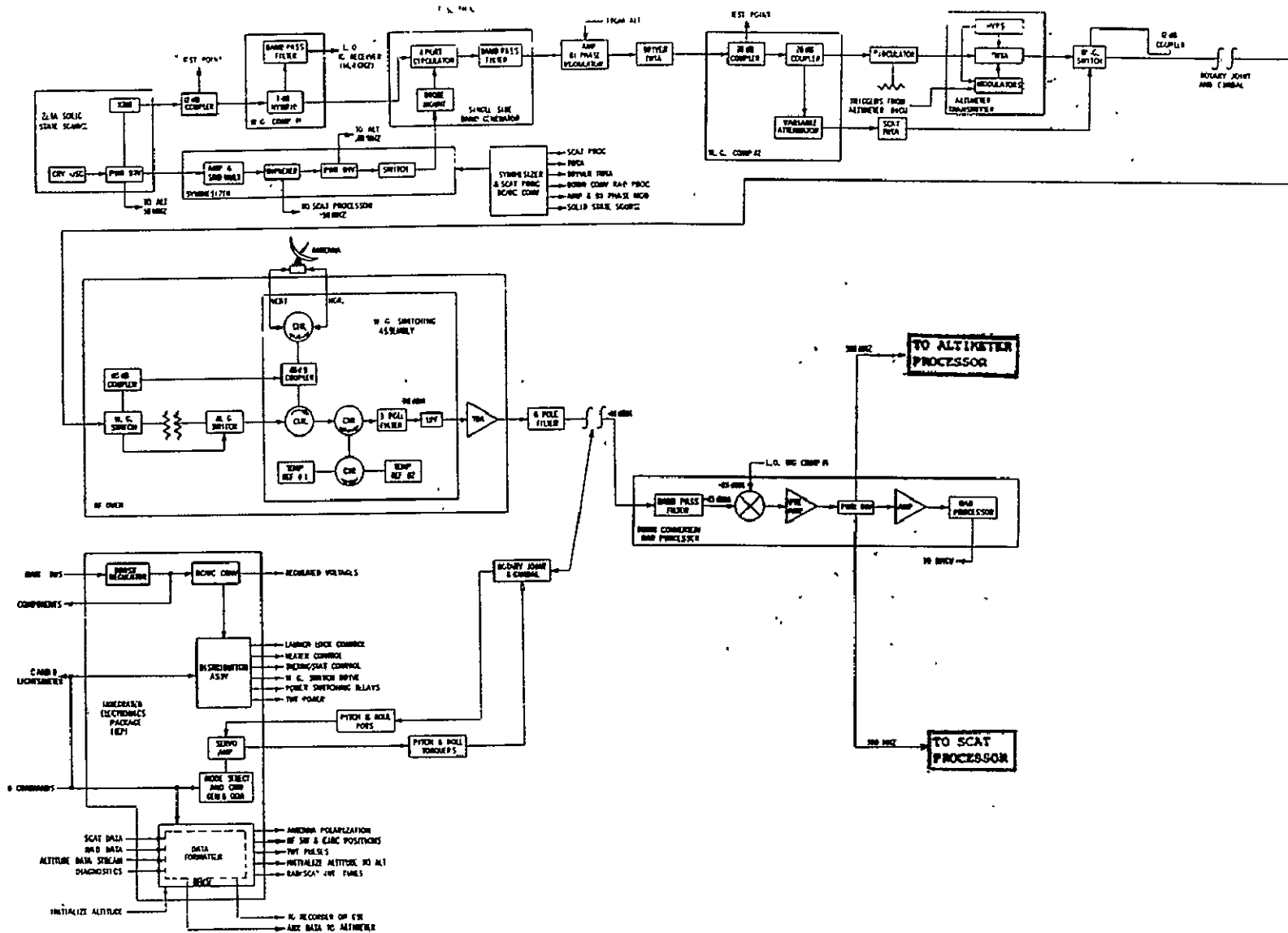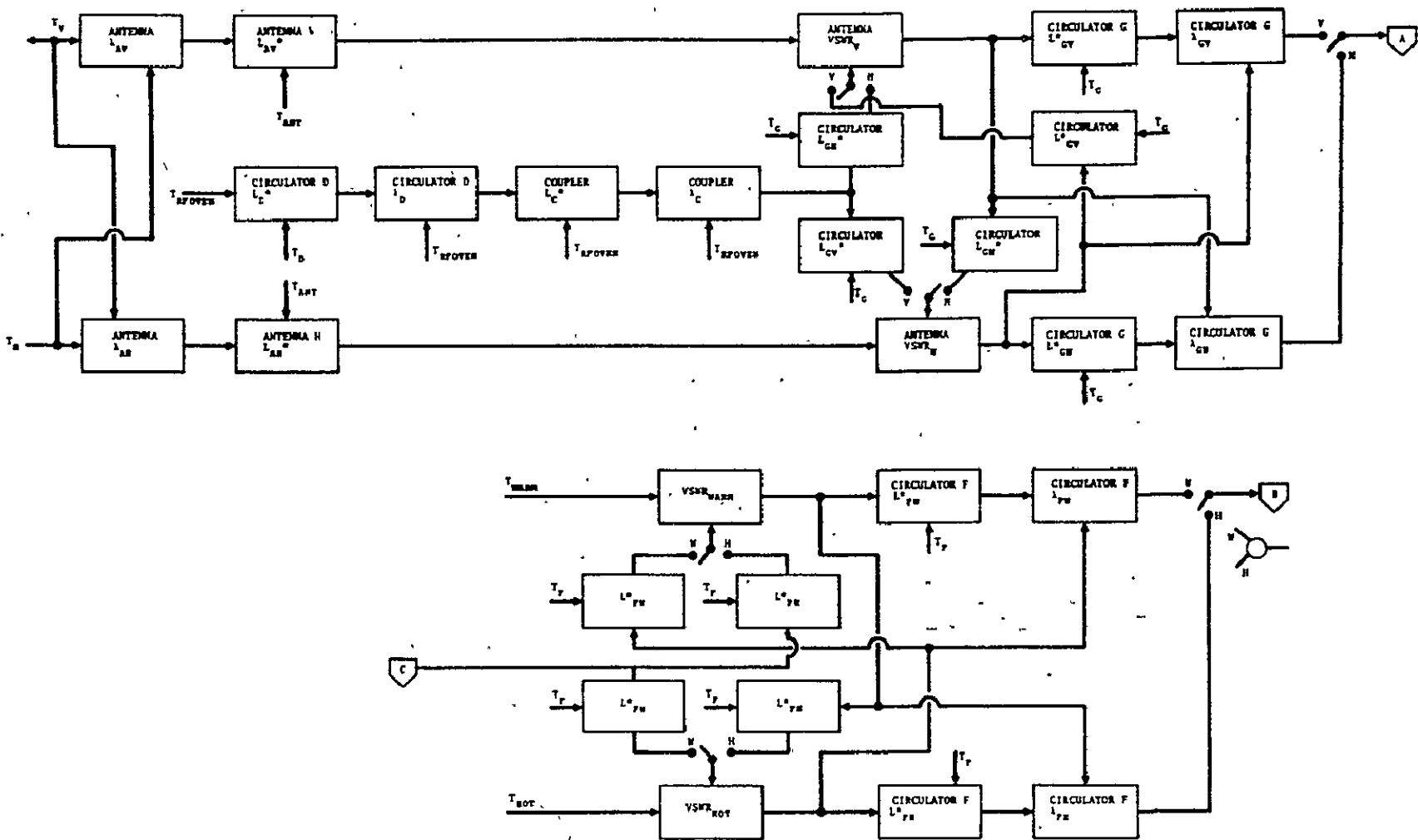
Figure 3. — S193 block diagram.

2-15

Figure 4. — S193 Radiometer element block diagram.

2-16
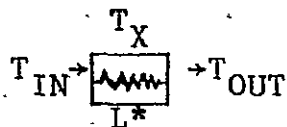
Figure 4. — S193 Radiometer element block diagram (concluded).

2-17
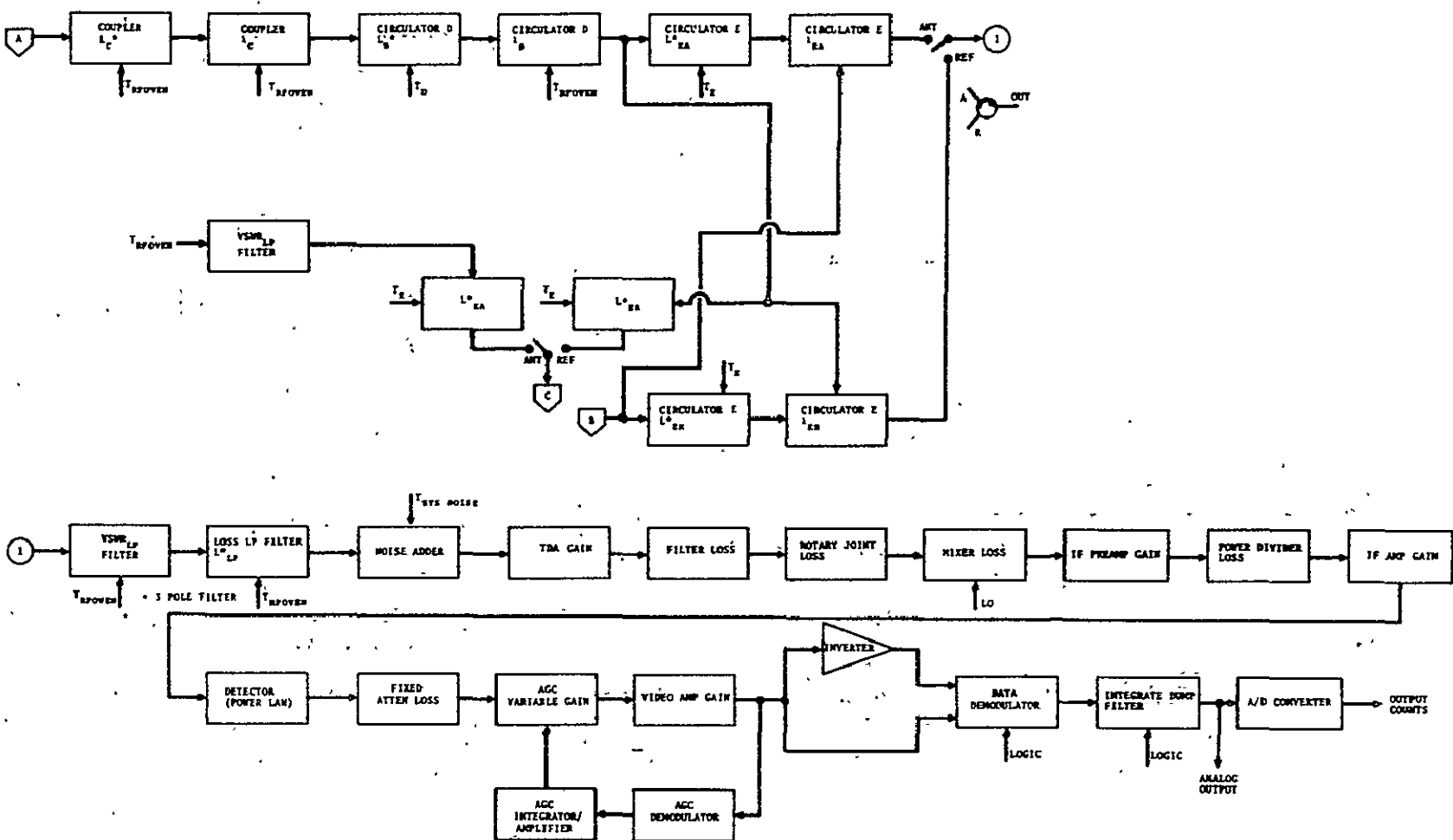
- Imperfect isolation (or leakage). (Also handles cross-polarization component)

- Reflections at discontinuities

- System noise generation

- Component gains

- Power law detection

- Analog to digital conversion.

The dissipative losses are handled in the model by using equation (16). A schematic representation of a lossy element is shown above the equation,

$$T_{OUT} = \frac{T_{IN}}{L^*} + T_X \frac{(L^* - 1)}{L^*} \tag{16}$$

where

T_{IN} = Input radiometeric temperature to the element.

T_{OUT} = Output radiometric temperature.

T_X = Thermal temperature of the lossy element.

L^* = Loss ratio of the dissipation loss (i.e., Power input/Power output) ≥ 1.0.

The imperfect isolation or leakage of the switches and other components, and the coupling of couplers is taken into account by equation (17).

$$T_{OUT} = T_{IN} (1 - \lambda) + \lambda T_{und} \tag{17}$$

where

T_{und} = Radiometric temperature input to the isolated
port.

λ = Coupling or leakage ratio (power output due to
isolated port).

The S193 antenna is fed by a dual polarization feed
structure. The power received through either the vertical
or horizontal port contains leakage power from the cross-
polarized port. The antenna has been modeled as an ideal
dual-polarized antenna followed by a mixing matrix. The
following assumptions are made:

1. The antenna is linear over the ranges of power
received as a radiometer, i.e., its properties
are independent of power received.

2. The ratios of mixing powers from one polarization
(V or H) to another (H or V) are constant.

3. The ratios of power mixing between polarizations
$(\lambda_{AV}, \lambda_{AH})$ are correct and have not changed since
the last measurement.

4. The vertical radiometric signals and horizontal
signals received are uncorrelated.

Based on the preceding assumptions, the following
equations calculate temperatures that include the effects
of cross-polarization:

$$T_{AV} = T_V(1 - \lambda_{AV}) + \lambda_{AV} T_H \qquad (18)$$

$$T_{AH} = T_V \lambda_{AH} + T_H(1 - \lambda_{AH}) \qquad (19)$$

where

T_V = Radiometric temperature of the vertically polarized radiation received at the aperture of the antenna.

T_H = Radiometric temperature of the horizontally polarized radiation received at the aperture of the antenna.

$\lambda_{AV}(\lambda_{AH})$ = Ratio of cross-polarized power to total power received, i.e., horizontal (or vertical respectively) when antenna is switched to vertical port, (or horizontal port respectively)

$T_{AV}(T_{AH})$ = Radiometric temperature in antenna's vertically polarized channel (or horizontally polarized channel respectively) after cross polarized energy has entered but before consideration of antenna loss.

The effects of reflection at a mismatched junction are described by:

$$T_{OUT} = T_{IN} \frac{4VSWR}{(VSWR + 1)^2} + T_R \left(\frac{VSWR - 1}{VSWR + 1}\right)^2 \qquad (20)$$

where

VSWR = Voltage Standing Wave Ratio at a mismatched junction, (e.g., the antenna-RF oven interface)

T_R = Radiometric temperature which is presented to the junction by the thermal radiation of components following the junction.

The tunnel diode amplifier and other front end components generate noise which is added to the incoming radiometric noise powers. This is handled by the computer model using the equation:

$$T_{NOISE} = T_{IN}' + T_{SYS} \tag{21}$$

where

T_{IN}' = Radiometric noise temperature in degrees Kelvin of the input as modified by the components preceding the tunnel diode amplifier

T_{SYS} = System noise temperature degrees Kelvin

T_{NOISE} = Output noise temperature of the receiver front end in degrees Kelvin.

Component gains are handled by a straight multipication of component power input by power gain to give power output.

The video detector in the system is nominally a square law detector. Expressed theoretically, the voltage output of the detector is directly proportional to the power input. The mathematical model for the detector follows:

$$V_{DET} = (P_{IN} + P_{OFF})^{BETA} \tag{22}$$

where

V_{DET} = Detector output voltage

P_{IN} = Power input to detector

BETA = Detector exponent divided by 2 (BETA = 1 for an ideal square law detector)

P_{OFF} = Offset power (set to 0 n the present model)

2-21

P_{OFF} is incorporated in the model to handle offsets which may occur in the detector. The parameter BETA can be varied to account for the deviations from square law in the detector.

A dc offset voltage is introduced into the model, via addition, to correspond to those offsets present in the actual system.

The analog to digital conversion for the radiometer model was programmed to use the 20 calibration points provided by General Electric to interpolate all 1023 levels for the 10-bit conversion.

Logic has also been included to automatically select certain paths and parameters as the signal goes through the polarization, calibration, and baseline functions. The integration times and modes of operation, etc., have been selected and are given in the S193 Calibration Data Report.

The final voltage output from the model is computed in the main program. The main program simulates the switching present in the S193 Radiometer processor from calibrate, to baseline, to antenna, etc. The parameter values used in the radiometer model are given in table I.

The computer model has been used to generate outputs (scientific data for vertical and horizontal polarization, calibration voltage, and baseline voltage) for several combinations of the model parameters with the input radiometric temperatures varied from 3°K for deep space to 300°K for hot targets.

TABLE I.– RADIOMETER PARAMETER VALUES

Computer Symbol Used In Model	Parameter Mathematical Symbol (see note 5)	Value	Comments
TV	T_V	3.0	1
TH	T_H	3.0	1
TANT	T_{ANT}	2.3665×10^2	3
TRFO	T_{RFO}	2.9775×10^2	2
THL	T_{HL}	3.922×10^2	2
TWL	T_{WL}	3.183×10^2	2
TD	T_D	2.9995×10^2	3
TE	T_E	2.9865×10^2	3
TF	T_F	2.992×10^2	3
TG	T_G	2.991×10^2	3
TSYS	T_{SYS}	1.180×10^3	
LSAV	L^*_{AV}	1.055626	
LSAH	L^*_{AH}	1.072161	
LSC	L^*_C	1.027845	
LC	λ_C	1.2148×10^{-4}	
LSD	L^*_D	1.048409	
LD	λ_D	9.1877×10^{-4}	

TABLE I.— RADIOMETER PARAMETER VALUES (Continued)

Computer Symbol Used In Model	Parameter Mathematical Symbol (see note 5)	Value	Comments
LSEA	L^*_{EA}	1.051869	
LSER	L^*_{ER}	1.051869	
LEA	λ_{EA}	3.5495×10^{-3}	
LER	λ_{ER}	3.5495×10^{-3}	
LSFH	L^*_{FH}	1.048532	
LSFW	L^*_{FW}	1.041436	
LFH	λ_{FH}	2.25527×10^{-4}	
LFW	λ_{FW}	1.092285×10^{-4}	
LSGV	L^*_{GV}	1.021855	
LSGH	L^*_{GH}	1.019385	
LGV	λ_{gv}	4.39×10^{-4}	
LGH	λ_{gh}	1.72×10^{-4}	
LSLP	L^*_{LP}	1.107962	
VSWRV	$VSWR_V$	1.262	
VSWRH	$VSWR_H$	1.262	
VSWRHL	$VSWR_{HL}$	1.045	
VSWRWL	$VSWR_{WL}$	1.0392	

TABLE I.— RADIOMETER PARAMETER VALUES (Concluded)

Computer Symbol Used In Model	Parameter Mathematical Symbol (see note 5)	Value	Comments
VSWRLP	$VSWR_{LP}$	1.0	
RIGAIN	RIGAIN	1.5715×10^{-2}	4
POFF	POFF	0.0	
BETA	BETA	1.0	
GVIDEO	GVIDEO	1.0	
EOB	E_{OB}	3.30×10^{-1}	
LAH	λ_{AH}	7.8412×10^{-2}	
LAV	λ_{AV}	6.145×10^{-2}	

1. Input data

2. Housekeeping data

3. Computed from housekeeping data

4. Gain factor (adjustable)

5. Symbols are defined in figure 4 or the preceding text.

2.6 Precision/Accuracy Data Processing

The simulation modeling required the capability for processing the simulated data. Consequently, a program which contains the data reduction equations used in TR524,[13] Earth Resources Production Processing Requirements for EREP Electronic sensors (without baseline and calibration value averaging) was developed. This program uses the same housekeeping values and data inputs necessary for production data processing. In order to allow use of this computer program as an analysis tool, the values of each parameter can be varied individually as desired. See appendix A for a description of the S193 production data processing.

3.0 S193 DATA FLOW

The basic flow of S193 data, shown in figure 5, has been abstracted from PHO-TR524[13]. The portions of section 6 of PHO-TR524 applicable to the radiometer have been completely reproduced in appendix A to facilitate defining the radiometer processing algorithm.
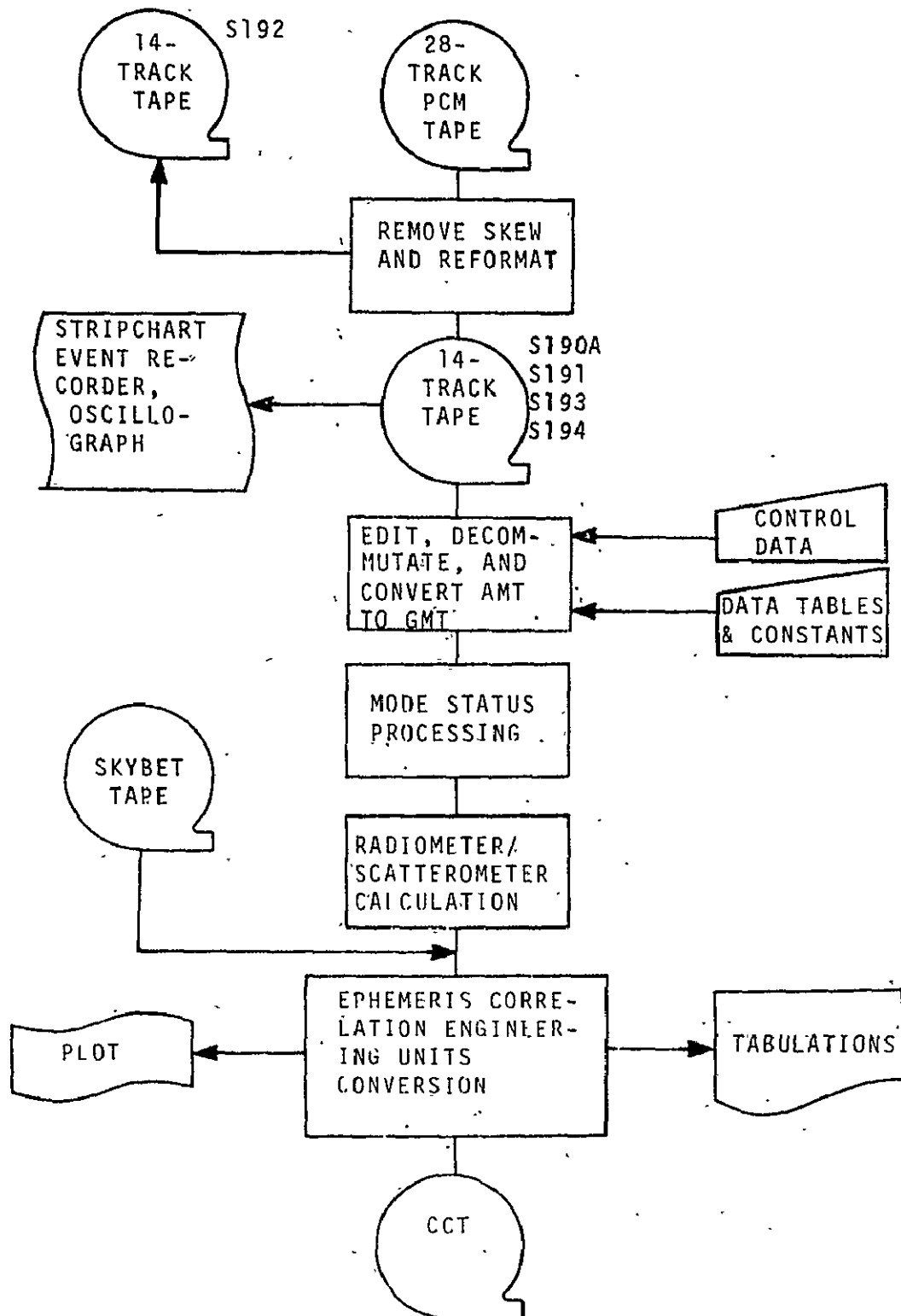
Figure 5. — S193RS processing flow.

4.0   OTHER EREP SENSORS

Two of the other four EREP sensors were used to aid in the evaluation of S193 data; the S194 L-band radiometer and the S190A camera system.

4.1   The S190A Camera System

The S190 camera system consists of six high-precision 70mm cameras with matched distortion and focal length. The lenses have a focal length of 6 inches, giving a 21.2° field-of-view across flats, which provides an approximately 80 nautical mile square of surface coverage on the earth from the Skylab orbit. Data from only one of the six cameras, i.e., station 4, which used high resolution color film, has been used in this evaluation.

4.2   The S194 L-Band Microwave Radiometer

The S194 L-band microwave radiometer was designed to make radiometric brightness temperature measurements in the 1.400 to 1.427 GHz radioastronomy band. The 1 meter square, 64-element planar array antenna was designed to have a half power beamwidth of 15° and a null-to-null beamwidth of approximately 36°. The beam efficiency was reported to be over 97 percent by the contractor. The broad beamwidth leads to a ground footprint area almost two orders of magnitude larger than the S193 footprint area. This difference in areas makes comparisons difficult. In many cases however, the S194 provides the only radiometric data for comparison with S193.

A further difficulty in comparison results from the limitation of a fixed mounting for S194. It is hard-mounted to always look at nadir when the spacecraft attitude is correct.

5.0 GROUND TRUTH SOURCES AND SENSORS

In order to assess the precision and accuracy of the
S193 Radiometer, ground truth from a number of sources has
been employed.

5.1 Meteorological Data

Meteorological data available over the sites has been
supplied by the U.S. Weather Bureau. In the case of the
Skylab 2 pass over the Great Salt Lake Desert, rainfall
data for 5 days prior to the pass was obtained from sur-
rounding stations.

5.2 Maps

Since the evaluation of precision and accuracy requires
large homogeneous targets, maps of the test sites were fre-
quently consulted to determine or verify the probable
homogeneity of the targets. For ocean targets, generally
Jet Navigation charts with scales of 1 to 2,000,000 or 1 to
3,000,000 were employed. For land targets, maps such as
sectional aeronautical charts with scales of 1 to 500,000
and various 1 to 250,000 scale maps were employed. In
special cases, 7-1/2-minute quadrangle maps with scales of
1 to 24,000 were consulted.

5.3 Supplementary Data

A small amount of other ground truth information was
obtained by consultation with geologists and other specialists
employed by NASA/JSC and Lockheed Electronics Company, Inc.

6.0 AIRBORNE SENSORS

6.1 Multifrequency Microwave Radiometer (MFMR)

The Multifrequency Microwave Radiometer (MFMR) consists of four individual radiometers mounted in the nose of the NASA P-3 aircraft. The radiometers are operated at frequencies of 1.42, 10.625, 22.235, and 31.4 GHz. Polarization can be horizontal, or vertical. The center of the sensors field-of-view from the aircraft can be varied from nadir to approximately 20° from zenith, i.e., zenith angles of 20° to 180°.

6.2 Metric Camera

On all flights in support of S193 sensor performance evaluation, a RC-8 metric camera which used 9-inch by 9-inch color film was used to supply a photographic record of the ground sites flown over. This camera is operated in a stabilized mount onboard the NASA P-3 aircraft. The camera uses a 6-inch lens with field-of-view of approximately 90°. The photography from this camera was available to aid in checking the test site homogeneity.

6.3 Laser Profiler

The Geodolite-3 laser profiler on board the P-3A was used to measure surface roughness. Time constraints have prevented evaluation of this data.

6.4 LTN-51 Inertial Navigation System

The LTN-51 inertial navigation system operates by sensing aircraft accelerations from a gyrostabilized, four gimbal all-attitude platform. The system output provides present position (longitude and latitude) information, course line computation, steering commands, and angular roll, pitch and heading information. As well as providing navigation information and commands to the pilot, it is used in determining wind velocity over the site. Information from the LTN-51 is especially useful in evaluating data from ocean targets.

7.0 DATA ANALYSIS PROCEDURES AND COMPARISON OF S193 RADIOMETER AND OTHER EXPERIMENTAL AND THEORETICAL RESULTS

Precision and accuracy must be estimated by comparison of S193 data with that from other sensors along with results from various models. For comparison purposes, target sites which have known properties capable of being modeled or have been measured by other instruments are required. In order to properly evaluate the system a variety of "cold," "warm", and "hot" targets are needed. The precision and accuracy evaluations depend upon "constant temperature targets." No target, except deep space, is constant in temperature but a number of targets come close enough to be of practical use in evaluating precision and accuracy.

The targets selected for this evaluation are given in table II. Results from the Great Salt Lake Desert proved to be disappointing and, in some cases, unusable because it was not a constant temperature target. In the quest for a suitable hot target, data form the Sahara Desert were tried. Results were good enough that the Sahara Desert has been added as a site for evolution of the SL3 instrument. Data from other sites have been added to give a more complete evaluation of precision.

7.1 Data Analysis Methods

7.1.1 Analysis With No Data Editing (Method 0). Method 0 (zero) for data analysis consisted of taking all the processed data (from PDP) for a particular site and, using the

computer to calculate a mean, median, mode, range, maximum
value, minimum value and standard deviation of the data,
tally the number of samples. For a truly "constant temper-
ature target" this method of data analysis will yield excel-
lent, unbiased results. Theoretically, the radiometer data
for a constant temperature target should form a Gaussian
(i.e., normal) distribution. The computer is also used to
generate empirical distribution plots and a fitted Gaussian
distribution curve as shown in figure 6.

In figure 6, notice that data points are present out
to 28.00°K even though this is over 8.5 standard deviations
from the mean. This data time slice obviously contains
data from a target other than the desired one. In this
particular case (from Lunar Cal I) the moon has appeared in
the main beam of the antenna in some measurements. Obviously,
this data has been biased upward and should be removed from
the analysis.

This illustrates the major weaknesses of Method 0. Data
from unwanted targets is accepted on an equal basis with the
desired target data biasing the mean and distorting the
standard deviation reported.

Two methods (called I and II) have been used to remove
data affected by unwanted targets for analysis, but neither
is perfect.

7.1.2 Analysis With Hand Data Editing (Method I).
Method I is a subjective hand analysis by the author which
varied slightly in form from target to target. For example,
in deep space before any computer analysis was available,

VERTICAL POLARIZATION WITH   1414 DATA POINTS

LARGEST VALUE =   27.99752188 SMALLEST VALUE =   7.13023496

START TIME 15/31/   12.0686 END TIME 15/34/   .23A5
PLOT OF NORMAL DISTRIBUTION

MEAN=   15.99405732   NO. OF OBSERVATIONS= 1414
VARIANCE=   2.50925145   NF. OF GROUPS= 22

CENTERPOINT OF INITIAL GROUP OF EMPIRICAL DENSITIES =   7.00000000
CENTERPOINT OF FINAL GROUP OF EMPIRICAL DENSITIES =   28.00000000
STEPSIZE=   1.00000000   K FACTOR= 3.

'E' IS THE PLOT SYMBOL FOR THE EMPIRICAL DENSITIES
'C' IS THE PLOT SYMBOL FOR THE CALCULATED DENSITIES
PERCENTAGE
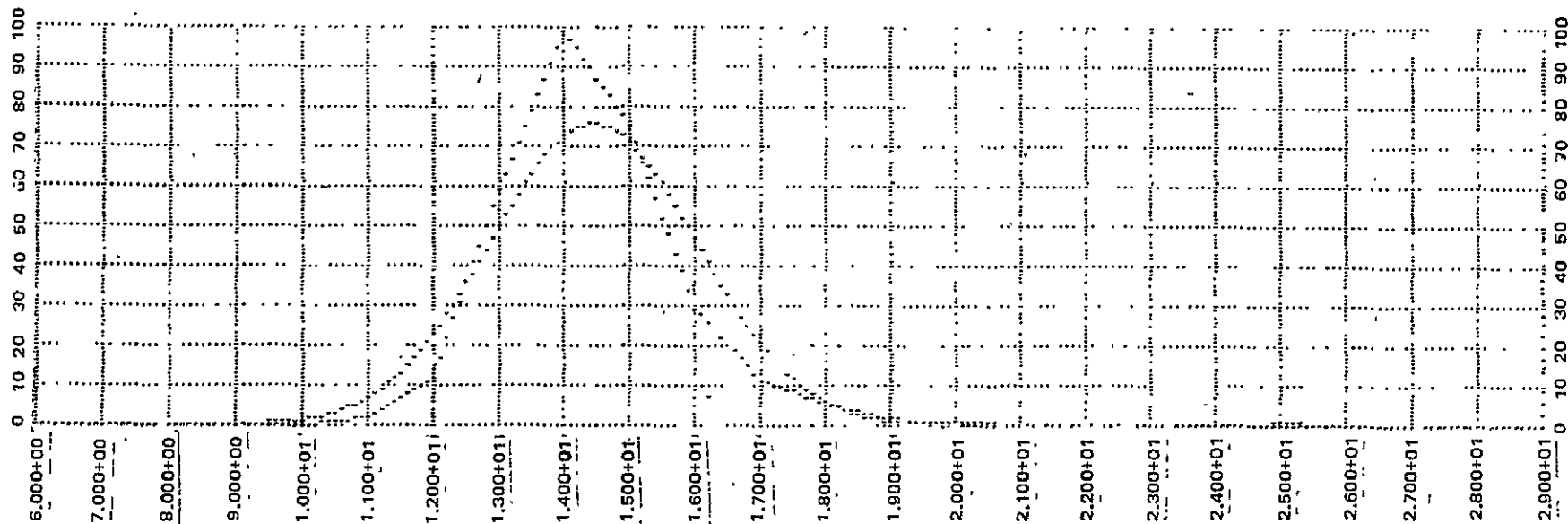
Figure 6. — Gaussian curve fit to unedited data.

the author examined the data making the assumption that radiometric temperature data which was affected by the moon's presence would appear to be biased upward in repeated scans across the moon. Therefore, plots of successive scans were examined for "spikes" appearing at similar role angles in successive scans. Using this procedure, data which appeared to be 2°K or more higher than surrounding measurements in repeated scans, was discarded before statistics were calculated.

This procedure has the advantage of allowing "intelligent" or "informed" removal of data. It has the disadvantage of being subject to the personal bias of the observer. If the observer discards too much data the radiometric temperature results will be too low, indicating a more accurate or precise performance than the instrument actually achieved.

Results from this analysis are shown in the tables of sections 7.2, 7.3, and 7.4. Since this analysis was performed by a manual search of the production data tabulations and plots, entries in these tables are not all complete.

When computer analysis of the data is available, this method takes the form of examing computer-plotted distributions for "wild" points which appear far from the mean and removing them by hand calculations from the statistics reported. For example, this type of correction of the data illustrated in figure 6 would have involved removal of all data above approximately 20°K; in particular, the data appearing at 25°K would have been removed as being affected by an unwanted radiating source.

7.1.3 Analysis With Computer Data Editing (Method II).
Method II, employed for removing biased radiometric data,
is as follows. The computer accepted all radiometric tem-
peratures for a particular scan mode and polarization
during a given time slice or within the desired geographic
area. The mean, median, mode, range and standard deviation
of these data points were computed. The minimum of the mean,
median and mode was selected as a test point (since the
method was developed for deep space data, the moon, as a
warm target, would bias the radiometric temperatures upward).
All points differing from the test point by more than 3 sam-
ple standard deviations of either larger or smaller values
are deleted. By deleting points both larger and smaller it
is hoped to avoid biasing the results by unsymmetrical
removal of valid data. The mean, median, mode, range, maxi-
mum and minimum are recomputed for this reduced set. The
experimental values are grouped into classes 1°K wide. The
distribution of this group is then plotted for comparison
with a Gaussian or normal distribution having the same mean
and variance. These plots are then examined for evidence
of significant deviations from a Gaussian distribution. For
example, if the empirical distribution appears to be multi-
modal, it is assumed that the target observed was not uniform.
In this case the entire data slice is either discarded or
further analysis on a reduced data set, by hand, is required.

This second procedure has the advantages of being objec-
tive in the editing of data and being performed automatically
by computer. It also preserves the symmetry of the distribu-
tion which would minimize any biases that might develop from
the procedure. However, it has the disadvantage of not
removing all the biased data.

Summary results of this computer analysis appear in the tables of sections 7.2, 7.3, and 7.4.

Examples of a data set before and after computer editing appear in figures 6 and 7. These show an example of an analysis considered successful by the author.

Figure 8 shows an example where the computer analysis failed. From an examination of 8, the author concluded that the sensor was observing a non-uniform target.

This type of computer analysis was performed for all sites noted in table II except Baja, California which was selected as a land-water interface target, and the Atlantic Ocean for which no data was analyzed.

7.1.4 <u>Selection of Best Analysis Method</u>. Where two or three analysis methods are employed on the same time slice of data, the author must judge which of the three most correctly represents the sensor's performance. In general, these selections have been made by examining the results for reasonableness, noting how well the mean, median, and mode coincide, and examining computer-generated distribution plots. Since these selections merely represent the author's professional judgment, condensed data from the other methods has been reported to allow the reader to make his own professional judgments.

7.1.5 <u>Correcting Estimates of Standard Deviation</u>. The number of data samples available for analysis varies from mode to mode and time slice to time slice over at least

Figure 7. — Gaussian curve fit to successfully edited data.

Figure 8. — Gaussian curve fit to unsuccessfully edited data.

7-8

TABLE II. — TARGET SITES FOR BRIGHTNESS TEMPERATURE PRECISION/ACCURACY

Site No.	Name	Coordinates Latitude - Longitude	Target Characteristics	Skylab Pass No.		
				SL2	SL3	SL4
749007	Deep Space		Field-of-view must exclude Sun and Earth but may include the Moon (Data with Moon in main beam discarded)	L-1	L-2 L-3	L-4 L-5
749598	Gulf of Mexico	20°00' - 30°00' N 82°00' - 97°00' W	Surface wind velocity - 25 knots No rain over target	5 8 11	12,13 15,16 20,36 44,46 52	No data analyzed
749233	Great Salt Lake Desert	41° N - 113°30' W (15 NM Radius)	No rain over target No surface water No vegetative land cover	5	12 16 37 39 40	No data analyzed
749691	North Atlantic Ocean (or other oceans)		No rain over target	No high sea state data acquired	No data analyzed	No data analyzed
749183	Baja, California		Land water interface	No data acquired	No data analyzed	No data analyzed
749855	Sahara Desert	20°00' - 25°00' N 00°00' - 07°00' W	No rain over target No surface water No vegetative land cover	No data acquired	21 22	No data analyzed

two orders of magnitude. Comparison of estimates of means
and standard deviations from 10 samples, on one hand, and
2900 on another will be misleading at best. In order to
make the comparisons as meaningful as possible it is neces-
sary to use unbiased estimators.

The sample mean, T_{mean} in equation (23), is an
unbiased estimator of the population mean.

$$T_{mean} = \frac{\sum\limits_{i=1}^{N} T_i}{N} \tag{23}$$

where T_i = the ith measurement of temperature.

It is also well-known that S^2, in equation (24), is
an unbiased estimator of the population variance:

$$S^2 = \sum_{i=1}^{N} \frac{\left(T_i - T_{mean}\right)^2}{N-1} \tag{24}$$

Common practice is to calculate the estimate of standard
deviation as being S. However, S is a biased estimator
of standard deviation. The bias becomes significant for
small samples.

It can be shown after considerable mathematical effort
that an unbiased estimate of standard deviation is:

$$\sigma_{est} = S \left[\frac{\Gamma\left(\frac{N}{2} - 1\right)}{\Gamma\left(\frac{N}{2} - \frac{1}{2}\right)} \cdot \sqrt{\frac{N-1}{2}} \right] \tag{25}$$

7-10

where

σ_{est} = Estimate of standard deviation.

$\Gamma(x)$ = Gamma function of X.

For computational convenience, the following approximation suggested by Dixon and Massey [14], has been employed:

$$\sigma_{est} = S \left[1 + \frac{1}{4(N-1)} \right] \qquad (26)$$

This approximation is correct within 0.3 percent for N=2 and improves rapidly as N becomes larger. The major restriction on this approximation is that the population be normally distributed, or nearly normally distributed. For a radiometer observing a constant, or nearly constant temperature target, this restriction is met.

The author knows the use of this correction factor applied to S is unusual. It has been introduced here to render comparisons of standard deviation between various sized samples more meaningful and to obtain more realistic estimates of precision and accuracy from the limited data available. Readers who prefer to work with S, as defined in equation (24), may simply divide the results presented in the tables to follow by the correction in brackets in equation (26).

7.2 SL2 Evaluations

To aid in the evaluation of targets, S190A color photographs are available. Photographic prints can be ordered from the EROS Data Center, Sioux Falls, South Dakota 57198.

Because of the fact that the color photographs from the S190A camera system utilized in this analysis are not easily reproduced; the following list, referencing photographs taken during SL2, was compiled.

THE SKYLAB 2 MISSION

Site Name	Skylab Pass No.	Magazine No.	Frame No.
Deep Space	LC 1	04	386-409
Gulf of Mexico	5	10	042-062
Gulf of Mexico	8	No S190A photographs over site	
Gulf of Mexico	11	04	292-311
Great Salt Lake Desert	5	10	001-014

Atmospheric conditions over the target sites during the SL2 mission are given in table III. Atmospheric conditions were supplied by the U.S. Weather Bureau.

7.2.1 <u>Deep Space Results from SL2</u>. During the LC-1 pass a number of radiometer modes were exercised. For deep space, a radiometric temperature of approximately 2.8°K is anticipated [5,6]. Webster [6] states that "The best and most recent value for the characteristic temperature of the radiation is 2.76 degrees K.; the measurements are so accurate that it is unlikely that this figure differs from the true one by more than 3 percent." Yet, it is believed that a figure of 2.8°K is good for this analysis.

During the LC-1 pass, the moon appeared in the antenna's main beam during some of the measurements. These biased

TABLE III. — ATMOSPHERIC CONDITIONS FOR SL2 TARGET SITES

Site Number	Site Name	Skylab Pass Number	Cloud Cover	Visibility	Pressure (MB)	Temp. (°F)	Dew Point	Winds	Sea Height (Ft)	Water Temp. (°F)
749598	Gulf of Mexico	5	6/10	N/A	N/A	80.6	24	12 knots from 90°	2	75.2
749598	Gulf of Mexico	8	6/10	N/A	N/A	82.4	24	11 knots from 90°	2	82.4
749598	Gulf of Mexico	11	4/10	N/A	N/A	82.4	24	14 knots from 130°	3	73.4
749233	Great Salt Lake Desert	5	Clear	20 mi.	1022	74.0	21	5 knots at 210° SSW	—	—

measurements must be removed to properly evaluate the data. The procedures described in 7.1 were used to remove affected data.

The data from Lunar Cal I are summarized in table IV.

The underlined data represents the author's professional judgment of which analysis method has provided results that are most representative of actual sensor performance without overstating the instrument's precision and accuracy. These judgments are based on consistency of results, anticipated performance of the instrument, and information available on target characteristics.

7.2.2. Gulf of Mexico Results from SL2. Table V gives a comparison of S193 measurements over water targets with values predicted by the smooth sea model of Paris[2,3,4] using the 1962 Standard Atmosphere. The values computed by Paris' model are considered to be lower bound values since brightness temperatures rise as the ocean roughness increases. The tolerance figures on Paris' model represent an estimated total uncertainty (i.e., bias error plus three standard deviations statistical error) in the model, in ground truth conditions, and in the antenna model used. The S194 data is taken using an antenna with a 16° field-of-view between half-power points oriented toward nadir.

7.2.3 Great Salt Lake Desert Results from SL2. Before the Skylab missions, the Great Salt Lake Desert was selected as a constant temperature hot target for sensor performance evaluation. However, the data from S193 demonstrates the

7-14

TABLE IV. — COMPARISON OF BRIGHTNESS TEMPERATURES MEASURED BY S193 WITH ACCEPTED VALUES AND S194 MEASUREMENTS FOR SL2

TASK SITE NAME AND NUMBER TIME	MODE	POL	IT (MSEC)	ANALYSIS TECHNIQUES	MEASURED BRIGHTNESS TEMPERATURE (S193) °K						NUMBER OF SAMPLES	ACCEPTED/S194 BRIGHTNESS TEMPERATURES	
					Mean	Median	Mode	Max.	Min.	Std. Dev.		Brightness Temp °K	Source
Deep Space 749007 Lunar Cal I (SL2) Start:165:15:44:43 Stop: 165:15:45:32	ITC R/S	V	32	0 I II	11.13 9.92 10.69	10.71 - 10.65	10.86 - 10.86	23.47 - 18.42	6.64 - 6.64	2.64 1.23 1.64	618 263 592	μ=2.8 0.5° Uncertainty	Literature (5,6)
Deep Space 749007 Lunar Cal I (SL2) Start:165:15:40:16 Stop: 165:15:42:10	CTC R/S	H	32	0 I II	12.71 12.71 12.79	13.00 - 13.01	13.10 - 13.10	18.23 - 18.23	4.34 - 6.03	2.27 2.27 2.14	643 643 636	μ=2.3° σ=0.5° max=4.1° min=2.2° 3548 Samples	S194 Data From SL2 LC-1 (15)
Deep Space 749007 Lunar Cal I (SL2) Start:165:15:42:12 Stop: 165:15:44:10	CTC R/S	V	32	0 I II	13.12 13.12 13.09	12.94 - 12.93	12.72 - 12.72	17.99 - 17.29	8.98 - 8.98	1.52 1.52 1.48	663 663 658		
Deep Space 749007 Lunar Cal I (SL2) Start:165:15:31:12 Stop: 165:15:36:00	CTC RAD	H	58	0 I II	13.90 13.79 13.86	13.75 - 13.75	13.68 - 13.68	20.81 - 18.40	7.77 - 10.01	1.58 1.43 1.46	1614 1568 1595		
		V	58	0 I II	14.45 14.36 14.35	14.28 - 14.27	14.12 - 14.13	28.00 - 18.84	7.13 - 9.43	1.58 1.32 1.28	1614 1586 1593		
Deep Space 749007 Lunar Cal I (SL2) Start:165:15:49:12 Stop: 165:15:49:58	ITNC R/S	H	* * * ** 256 128 58	0 I II I I I I	12.79 12.58 12.79 12.17 11.68 12.76 14.72	13.02 - 13.02 - - - -	14.50 - 14.50 - - - -	15.79 15.46 15.79 15.46 14.50 15.19 15.46	8.18 8.18 8.18 8.18 8.18 10.30 13.98	2.38 2.32 2.38 - 2.83 1.84 1.31	15 14 15 - 6 6 2		

7-16

TASK SITE NAME AND NUMBER TIME	MODE	POL	IT (MSEC)	ANALYSIS TECHNIQUES	MEASURED BRIGHTNESS TEMPERATURE (S193) °K Mean	Median	Mode	Max.	Min.	Std. Dev.	NUMBER OF SAMPLES	ACCEPTED/S194 BRIGHTNESS TEMPERATURES Brightness Temp °K	Source
Deep Space 749007 Lunar Cal I (SL2) Start:165:15:49:12 Stop. 165:15:49:58	ITNC R/S	\	*	0	12.79	13.01	13.50	15.50	8.76	2.13	14		
			*	I	12.79	-	-	15.50	8.76	2.13	14		
			*	II	12.79	13.01	13.50	15.50	8.76	2.13	14		
			**	I	12.52	-	-	15.50	8.76	-	-		
			256	I	12.52	-	-	15.04	8.76	2.61	6		
			128	I	12.55	-	-	14.37	9.81	1.76	6		
			58	I	14.97	-	-	15.50	14.44	0.94	2		
Deep Space 749007 Lunar Cal I (SL2) Start:165:15 52·04 Stop. 165:15:54·40	CTNC R/S	H	*	0	10.09	10.01	10.11	14.85	6.23	1.98	50	L=2.8° 0.5° Uncertainty	Literature (5,6)
			*	I	10.09	-	-	14.85	6.23	1.98	50		
			*	II	10.09	10.01	10.11	14.85	6.23	1.98	50		
			**	I	9.74	-	-	14.85	6.23	-	-		
			256	I	9.18	-	-	12.00	6.23	1.61	20		
			128	I	10.55	-	-	14.85	7.37	2.25	21	u=2.3° σ=0.5° Max=4.1° Min=2.2° 3548 Samples	S194 Data From SL2 LC-1 (15)
			58	I	11.03	-	-	12.61	8.80	1.48	9		
		V	*	0	12.16	12.39	13.17	15.82	7.79	1.80	50		
			*	I	12.16	-	-	15.82	7.79	1.80	50		
			*	II	12.16	12.39	13.17	15.82	7.79	1.80	50		
			**	I	12.01	-	-	15.82	7.79	-	-		
			256	I	11.83	-	-	14.37	7.79	1.77	20		
			128	I	12.19	-	-	15.82	8.52	2.15	21		
			58	I	12.81	-	-	14.23	11.12	0.98	9		
Deep Space 749007 Lunar Cal I (SL2) Start.165 15:50;30 Stop: 165.15:51:19	CTNC R/S	H	*	0	10.18	10.13	8.10	15.40	7.11	2.51	16		
			*	I	-	-	-	-	-	-	-		
			*	II	9.83	10.03	8.10	13.82	7.11	2.14	15		
			**	I	-	-	-	-	-	-	-		
		V	*	0	11.52	11.16	13.06	15.92	8.24	2.10	16		
			*	I	-	-	-	-	-	-	-		
				II	11.52	11.16	13.06	15.92	8.24	2.10	16		

*Unweighted average of all measurements in this node.
**Average weighted by total integration time.

7-17

TABLE V. — COMPARISON OF BRIGHTNESS TEMPERATURES MEASURED BY
S193 WITH S194 MEASUREMENTS AND SMOOTH SEA MODEL VALUES FOR SL2

TASK SITE NAME AND NUMBER TIME	MODE	POL	ANGLE OF INCI- DENCE (DEG)	ANALYSIS TECHNIQUE	MEASURED BRIGHTNESS TEMPERATURE (S193) °K						NUMBER OF SAMPLES	MODEL/S194 BRIGHTNESS TEMPERATURE	
					Mean	Median	Mode	Max	Min	Std Dev		Brightness Temp °K	Source
Gulf of Mexico 749598 Pass 5 Start:156:18:2:10 Stop :156:18:4:55	ITNC R/S	H	44-55	0/II	100.73	100.76	100.50	102.80	92.29	1.48	7	90±8	Paris (2,3,4)
			36-44	0/II	107.65	107.08	106.95	113.09	105.93	2.33	8	101±5	
			27-33	0/II	115.20	115.29	115.00	116.23	114.17	0.71	7	111±5	
			13-18	0/II	121.91	121.84	121.50	123.30	120.72	0.93	7	119±5	
			0-3	0/II	127.17	127.21	127.50	128.22	125.89	0.86	8	123±5	
		V	44-55	0/II	170.61	170.30	170.00	172.12	169.06	1.19	7	175±8	
			36-44	0/II	159.15	159.23	159.00	159.69	158.45	0.53	7	154±5	
			27-33	0/II	142.82	142.37	142.00	145.41	140.93	1.51	7	138±5	
			13-18	0/II	130.83	131.28	131.17	131.82	128.62	1.13	7	127±5	
			0-3	0/II	129.31	129.17	129.00	131.09	127.52	1.05	8	123±5	
Gulf of Mexico 749598 Pass 8	ITNC R/S	H	49-55	0/II	119.72	118.22	-	135.61	105.84	13.00	5	91±8	Paris (2,3,4)
			40-45	0/II	120.32	122.30	-	133.45	109.30	9.58	7	98±5	
			29-33	0/II	124.48	120.00	-	138.79	115.00	9.89	7	110±5	
			13-18	0/II	128.38	125.69	124.00	141.16	122.20	7.54	6	121±5	
			0-3	0/II	130.22	128.67	-	136.19	127.32	4.37	4	124±5	
		V	49-55	0/II	183.08	182.93	-	192.00	173.51	8.18	5	176±8	
			40-45	0/II	170.18	172.60	173.00	180.48	159.08	8.33	7	162±5	
			29-33	0/II	153.05	151.75	-	164.34	141.92	9.52	7	139±5	
			13-18	0/II	137.22	136.25	140.00	150.28	129.95	9.74	6	128±5	
			0-3	0/II	132.55	131.64	-	138.08	128.84	4.25	4	124±5	
												μ=90.5 σ= 1.7 max=96.6 min=89.2 411 samples	S194 Data From Pass 8 (15)

TABLE V. — COMPARISON OF BRIGHTNESS TEMPERATURES MEASURED BY
S193 WITH S194 MEASUREMENTS AND SMOOTH SEA MODEL VALUES FOR SL2 (CONCLUDED)

TASK SITE NAME AND NUMBER TIME	MODE	POL	ANGLE OF INCI-DENCE (DEG)	ANALYSIS TECHNIQUE	MEASURED BRIGHTNESS TEMPERATURE (S193) °K						NUMBER OF SAMPLES	MODEL/S194 BRIGHTNESS TEMPERATURE	
					Mean	Median	Mode	Max	Min	Std Dev		Brightness Temp °K	Source
Gulf of Mexico 749598 Pass 11 Start:165:14:48:32 Stop :165:14:49:31	ITC R/S	H	44-55	0/II	122.41	122.85	123.13	126.74	117.73	2.56	48	90±8	Paris (2,3,4)
			36-44	0/II	125.29	125.90	127.65	130.06	118.47	2.78	81	100±5	
			28-36	0/II	128.23	128.59	128.13	133.19	122.41	2.62	62	110±5	
			8-16	0/II	133.04	133.19	133.45	137.07	128.14	1.87	126	120±5	
			0-8	0/II	133.74	133.86	133.81	136.65	128.89	1.63	135	122±5	
Gulf of Mexico 749598 Pass 11 Start:165:47:41 Stop :165:48:27	ITC R/S	V	0-5	0/II	204.62	206.27	211.79	213.45	189.50	6.72	59	122±5	Paris (2,3,4)
			12-16	0/II	201.54	202.72	210.71	212.22	189.50	7.21	52	126±5	
			29-33	0/II	204.63	205.77	195.90	217.17	189.56	8.37	22	138±5	
			38-42	0/II	205.84	205.74	206.10	220.28	191.02	8.92	34	153±5	
			44-48	0/II	201.41	201.53	205.78	207.17	196.26	4.36	24	165±8	
												μ=90.2 σ=2.2 Max=103.7 Min=88.0 333 Samples	S194 Data From Pass 11

Great Salt Lake Desert is not a constant temperature target.
This is vividly demonstrated in figure 9 where S193 measure-
ments have been assigned to 0.1° squares of latitude and
longitude by the center of the calculated field-of-view.

Notice that a brightness temperature range of over 70°K
is encountered. It may also be noted that this is the data set
illustrated in figure 8 where the computer analysis failed.

Unfortunately, this Great Salt Lake Desert data is not
usable for precision/accuracy analysis. This data indicates
that a potential application for microwave data exists for
measuring the soil properties which are causing the high
variance of measurements. The target properties causing the
response are unknown at present; however, soil moisture and/or
salt content seem to be likely candidates.

7.2.4 Other Land Target Results from SL2. In order to
partially overcome the failure of the Great Salt Lake Desert
as a constant temperature site, a number of S193 data takes,
near the end of SL2, were examined. Those which show the
characteristics of constant temperature targets are pre-
sented in table VI. No ground truth information was avail-
able for these sites.

7.3 SL3 Evaluation

During the Skylab 3 mission, the following S190A photog-
raphy of, or near the evaluation sites, was acquired.
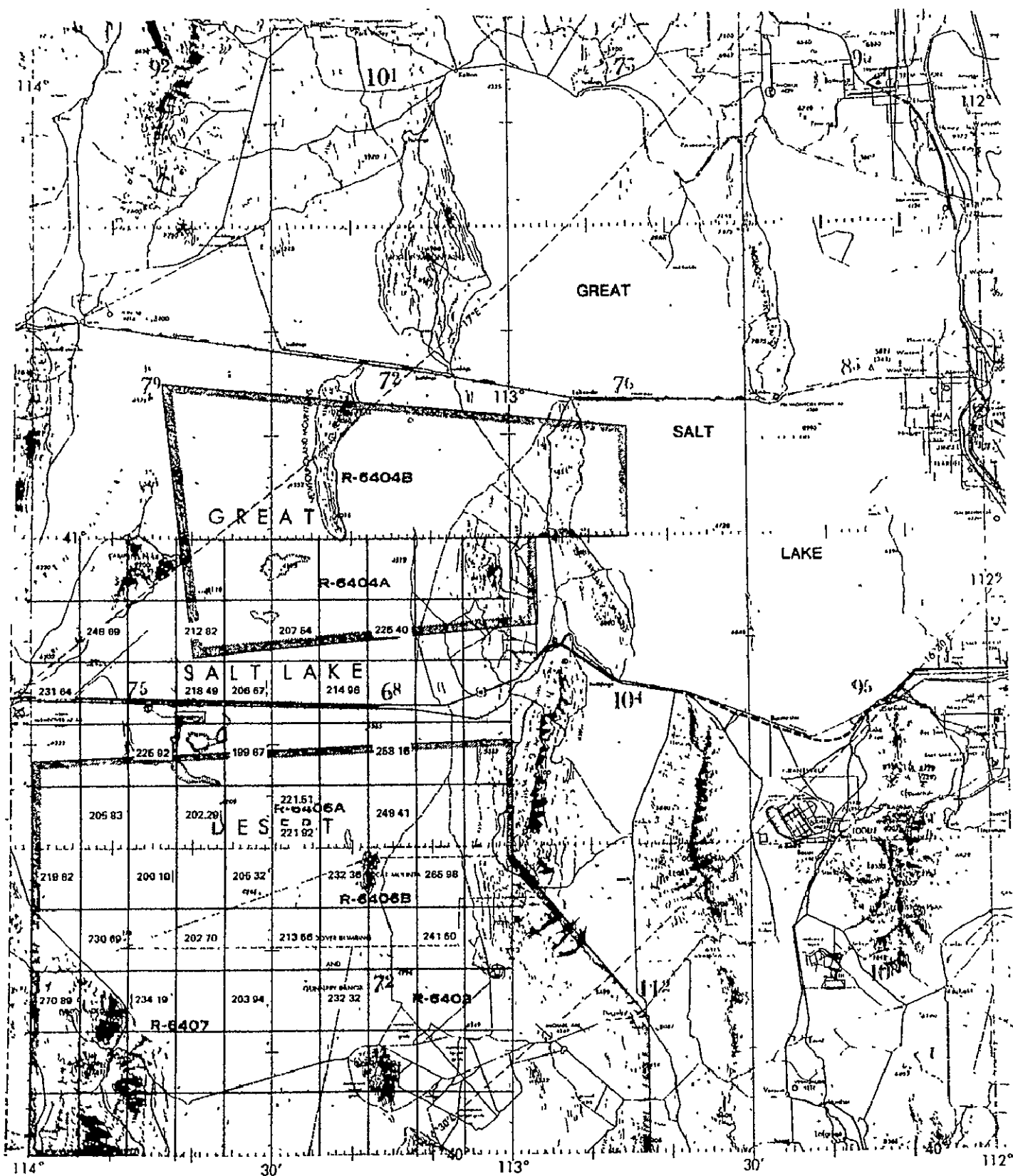
Figure 9. — S193 measurements over Great Salt Lake desert pass 5.

TABLE VI. — BRIGHTNESS TEMPERATURES MEASURED BY S193 OVER SELECTED LAND TARGETS

TASK SITE NAME AND NUMBER TIME	MODE	POL	IT (MSEC)	ANALYSIS TECHNIQUE	MEASURED BRIGHTNESS TEMPERATURE (S193) °K						NUMBER OF SAMPLES
					MEAN	MEDIAN	MODE	MAX	MIN	STD DEV	
Washington Idaho, Montana Pass 10 Start 164:13:46:10 Stop 164:13:46:26	ITNC	H	*	0/II	259.60	260.16	261.00	262.93	256.13	2.48	10
Washington. Idaho Montana, Wyoming Pass 10 Start 164:13:48:31 Stop 164:13:48:51	ITNC	V	*	0/II	268.43	270.16	264.00	272.78	263.54	4.08	12
Brazil Pass 10 Start 164:14:11:17 Stop 164:14:11:46	CTC R/S	H **	32	0/II	277.85	277.56	277.56	282.98	271.37	2.28	167
Brazil Pass 10 Start 164:14:11:49 Stop 164:14:12:17	CTC R/S	V **	32	0 I	274.85 274.60	274.74 -	274.32 274.32	280.06 280.06	263.69 ≈266.50	2.26 2.09	161 160

*All samples were equally weighted regardless of integration time.

**Polarization is defined in terms of the sensor's selected input parts. For crosstrack modes, this does not correspond to the polarization incident at the target.

Site Name	Skylab Pass No.	Magazine No.	Frame No.
Deep Space	L-2	28	280-297
Deep Space	L-3	34	329-334
Gulf of Mexico	13	22	117-149
Gulf of Mexico	16	22	336-362
Gulf of Mexico	20	28	201-244
Great Salt Lake Desert	12	22	001-015[1]
Great Salt Lake Desert	16	22	305-350

Atmospheric conditions over the SL3 sites are given in table VII. Atmospheric conditions were supplied by the U.S. Weather Bureau.

7.3.1 Deep Space Results from SL3. During SL3, the Lunar Cal II and Lunar Cal III passes were made when a number of radiometer modes were exercised. The S193 radiometer data from these two passes are summarized in tables VIII and IX.

The underlined data represents the author's professional judgment of which analysis method has provided results that are most representative of actual sensor performance without overstating the instruments precision and accuracy.

7.3.2 Gulf of Mexico Results from SL3. Table X gives a comparison of S193 measurements over water targets with the lower bound values predicted by the smooth sea model of Paris[2,3,4] with the 1962 Standard Atmosphere. The values

---

[1]S190A photographs are in proximity of site. No photographs taken over site.

TABLE VII. — ATMOSPHERIC CONDITIONS FOR SL3 TARGET SITES

Number	Name	Skylab Pass Number	Cloud Cover	Visibility	Pressure (MB)	Temp. (°F)	Dew Point	Winds	Sea (Ft)	Water Temp. (°F)
749598	Gulf of Mexico	13	Overcast (Precipitation)	N/A	1019	81	75	8 knots from 130°	2	86
749598	Gulf of Mexico	16	3/10	N/A	1018	87	74	10 knots from 90°	2	85
749598	Gulf of Mexico	20	5/10	N/A	1016	82	76	12 knots from 130°	4	87
749233	Great Salt Lake Desert	12	Scattered at 11,000 ft.	35 mi	1014	83	47	4 knots from 110°	-	-
749233	Great Salt Lake Desert	16	Clear	60 mi	1019	78	39	7 knots from 80°	-	-
749855	Sahara Desert	21	Clear	N/A	1004	107	50	Calm	-	-
749855	Sahara Desert	22	Clear	N/A	1011	104	40	5 knots from 110°	-	-

7-24

TABLE VIII. — COMPARISON OF BRIGHTNESS TEMPERATURES MEASURED BY
S193 WITH ACCEPTED VALUES AND S194 MEASUREMENTS FOR SL3

TASK SITE NAME AND NUMBER TIME	MODE	POL	IT	ANALYSIS TECHNIQUE	MEASURED BRIGHTNESS TEMPERATURE (S193) °K						NUMBER OF SAMPLES	ACCEPTED/S194 BRIGHTNESS TEMPERATURES	
					Mean	Median	Mode	Max	Min	Std Dev		Brightness Temp °K	Source
Deep Space 749007 Lunar Cal II Start:224:15:49.35 Stop :224:15:50:32	ITC R/S	V	32	0 / I / II	17.93 / 17.13 / 17.52	17.50 / - / 17.42	17.35 / - / 17.35	28.32 / 19.69 / 24.85	12.50 / 13.05 / 12.50	2.58 / 1.55 / 1.77	680 / 578 / 649	2.8° / 0.5° Uncertainty	Literature (5,6)
Deep Space 749007 Lunar Cal II Start:224:15:45:16 Stop :225:15:47:11	CTC R/S	H	32	0 / I / II	17.20 / 17.20 / 17.22	17.22 / - / 17.24	17.69 / - / 17.69	22.42 / 22.42 / 22.42	11.17 / 11.17 / 12.51	1.75 / 1.75 / 1.72	648 / 648 / 646	μ=2.3 σ=0.5 Min=2.2 Max=4.1 3548 Samples	S194 Data From SL-2 LC-1 (15)
Deep Space 749007 Lunar Cal II Start:224:15:47:10 Stop :224:15:49:10	CTC R/S	V	32	0 / I / II	14.90 / 14.91 / 14.89	14.78 / - / 14.76	14.69 / - / 14.69	19.35 / 19.09 / 19.07	10.71 / 10.71 / 10.71	1.47 / 1.51 / 1.47	660 / 656 / 659	μ=3.4 σ=0.3 Max=3.8 Min=3.0 2889 Samples	S194 Data From SL-4 LC-4(15)
Deep Space 749007 Lunar Cal II Start:224:15:36:12 Stop :224:15:41:01	CTC RAD	H	58	0 / I / II	16.04 / 15.79 / 15.93	15.85 / - / 15.83	15.41 / - / 15.41	31.13 / - / 20.35	12.44 / - / 12.44	1.72 / 1.25 / 1.34	1602 / 1439 / 1582		
		V	58	0 / I / II	16.44 / 16.14 / 16.38	16.20 / - / 16.18	16.03 / - / 16.03	24.88 / - / 20.90	12.13 / - / 12.13	1.65 / 1.52 / 1.51	1600 / 1423 / 1580		
Deep Space 749007 Lunar Cal II Start:224:15:54:01 Stop :224:15:54:50	ITNC R/S	H	* / * / * / ** / 256 / 128 / 58	0 / I / II / I / I / I / I	10.05 / 10.06 / 10.05 / 9.96 / 9.96 / 9.79 / 11.29	9.85 / - / 9.85 / - / - / - / -	10.10 / - / 10.10 / - / - / - / -	11.35 / 11.35 / 11.35 / 11.35 / 10.89 / 11.10 / 11.35	8.97 / 8.54 / 8.98 / 8.54 / 8.54 / 8.98 / 11.23	0.80 / 0.85 / 0.80 / - / 0.61 / 0.86 / 0.11	16 / 15 / 16 / - / 6 / ? / 2	μ=3.1 σ=0.3 Max=3.5 Min=2.6 2886 Samples	S194 Data From SL-4 LC-5 (15)

TABLE VIII. — COMPARISON OF BRIGHTNESS TEMPERATURES MEASURED BY
S193 WITH ACCEPTED VALUES AND S194 MEASUREMENTS FOR SL3 (CONCLUDED)

TASK SITE NAME AND NUMBER TIME	MODE	POL	IT	ANALYSIS TECHNIQUE	MEASURED BRIGHTNESS TEMPERATURE (S193) °K						NUMBER OF SAMPLES
					Mean	Median	Mode	Max	Min	Std Dev	
Deep Space 749007 Lunar Cal II Start:224:15:54:01 Stop :224:15:54:50	ITNC R/S	V	*	0	10.66	10.59	11.10	13.87	8.54	1.50	15
			*	I	10.66	-	-	13.87	8.54	1.50	15
			*	II	10.66	10.59	11.10	13.87	8.54	1.50	15
			**	I	10.62	-	-	13.87	8.54	-	-
			256	I	10.94	-	-	12.12	9.54	-1.13	6
			128	I	9.76	-	-	11.20	8.54	1.15	7
			58	I	13.00	-	-	13.87	12.12	1.54	2
Deep Space 749007 Lunar Cal II Start 224:15:55:16 Stop :224:15:57:16	CTNC R/S	H	*	0	9.62	9.48	9.50	14.22	6.45	1.83	38
			*	I	9.62	-	-	14.22	6.92	1.83	38
			*	II	9.62	9.48	9.50	14.22	6.45	1.83	38
			**	I	9.22	-	-	14.22	6.92	-	-
			256	I	8.96	-	-	10.94	6.99	1.18	15
			128	I	9.12	-	-	10.69	6.92	1.26	16
			58	I	12.17	-	-	14.22	8.50	2.07	7
		V	*	0	11.68	11.62	11.68	16.21	8.55	1.60	38
			*	I	11.68	-	-	16.21	9.28	1.60	38
			*	II	11.68	11.62	11.68	16.21	8.55	1.60	38
			**	I	11.47	-	-	16.21	9.28	-	-
			256	I	11.52	-	-	12.90	9.34	1.04	15
			128	I	10.92	-	-	13.18	9.28	1.16	16
			58	I	13.76	-	-	16.21	11.75	1.90	7

*Unweighted average of all measurements in this mode.

**Average weighted by total integration time.

7-26

TABLE IX. — COMPARISON OF BRIGHTNESS TEMPERATURES MEASURED BY
S193 WITH ACCEPTED VALUES AND S194 MEASUREMENTS FOR SL3

TEST SITE NAME AND NUMBER TIME	MODE	POL	IT (MSEC)	ANALYSIS TECHNIQUE	MEASURED BRIGHTNESS TEMPERATURE (S193) °K						NUMBER OF SAMPLES	ACCEPTED/S194 BRIGHTNESS TEMPERATURE	
					Mean	Median	Mode	Max	Min	Std Dev		Brightness Temp °K	Source
Deep Space 749007 Lunar Cal III Start:254:13.57.11 Stop :254:13:58:01	ITC R/S	\	32	0 II	19.57 19.57	19.52 19.52	19.52 19.52	25.13 24.63	13.92 14.68	1.79 1.77	621 619	2.8°K 0.5°K Uncertainty	Literature (5,6)
Deep Space 749007 Lunar Cal III Start:254:13:53:10 Stop :254:13:54.01	CTC R/S	H	32	0 I II	14.18 13.97 14.18	14.22 - 14.22	14.85 - 14.85	19.47 17.80 19.47	7.70 7.70 7.70	2.19 2.65 2.19	335 313 335	μ=2.3 σ=0.5 MAX=4.1 MIN=2.2 3548 Samples	S194 Data From SL-2 LC-1
Deep Space 749007 Lunar Cal III Start:254:13:53:10 Stop :254:13.54:01	CTC R/S	V	32	0 I II	14.47 14.24 14.45	14.55 - 14.55	14.87 - 14.87	20.17 16.87 19.36	9.61 9.61 9.61	1.73 1.61 1.70	288 263 287	μ=3.4 σ=0.3 Max=3.8 Min=3.0 2889 Samples	S194 Data From SL-4 LC-4 (25)
Deep Space 749007 Lunar Cal III Start: 254:13:46:14 Stop :254:13:48:27	CTC RAD ONLY	H	58	0 I II	14.20 13.92 14.20	14.01 - 14.01	13.85 - 13.85	17.99 17.81 17.82	9.82 10.79 9.82	1.37 1.20 1.36	740 644 739		
		V	58	0 I II	14.15 13.87 14.11	14.01 - 13.99	13.96 - 13.96	19.92 16.76 18.06	10.98 10.98 10.98	1.38 1.13 1.32	740 650 734	μ=3.1 σ=0.3 Max=3.5 Min=2.6 2886 Samples	S194 Data From SL-4 LC-5 (15)
Deep Space 749007 Lunar Cal III Start:254:13:48:52 Stop :254:13:49:56	ITNC R/S	H	* * * ** 256 128 S8	0 I II I I I I	7.49 7.49 7.49 7.30 7.42 6.60 10.37	7.78 - 7.78 - - - -	8.17 - 8.17 - - - -	12.76 12.76 12.76 12.76 8.73 8.28 12.76	3.65 3.65 3.65 3.65 5.44 3.65 7.68	2.03 2.03 2.03 - 1.39 1.68 2.87	21 21 21 - 9 9 3		

TABLE IX. — COMPARISON OF BRIGHTNESS TEMPERATURES MEASURED BY
S193 WITH ACCEPTED AND S194 MEASUREMENTS FOR SL3 (CONCLUDED)

TEST SITE NAME AND NUMBER TIME	MODE	POL	IT (MSEC)	ANALYSIS TECHNIQUE	MEASURED BRIGHTNESS TEMPERATURE (S193) °K					Std Dev	NUMBER OF SAMPLES	ACCEPTED/S194 BRIGHTNESS TEMPERATURE	
					Mean	Median	Mode	Max	Min			Brightness Temp °K	Source
Deep Space 749007 Lunar Cal III Start:254:13:48:52 Stop :254:13:49:56	ITNC R/S	V	*	0	6.85	6.98	7.00	12.96	4.50	1.91	21		
			*	I									
			*	II	6.55	6.78	7.00	9.11	4.50	1.32	20		
			**	I	6.51	-	-	12.96	4.50	-	-		
			256	I	6.35	-	-	7.76	4.50	1.25	9		
			128	I	6.27	-	-	8.22	4.73	1.15	9		
			58	I	10.08	-	-	12.96	8.18	2.85	3		
Deep Space 749007 Lunar Cal III Start: 254:13:58:28 Stop : 254:13:59:17	CTNC	H	*	0	9.97	9.99	9.07	12.94	7.42	1.53	15		
			*	I	9.97	-	-	12.94	7.43	1.53	15		
			*	II	9.97	9.99	9.07	12.94	7.42	1.53	15		
			**	I	9.66	-	-	12.94	7.43	-	7		
			256	II	9.38	-	-	11.17	7.43	1.45	7		
			128		9.94	-	-	11.82	8.71	1.26	6		
			58	I	12.12	-	-	12.94	11.29	1.46	2		
		V	*	0	11.39	10.98	11.00	15.02	8.18	1.76	16		
			*	I	11.66	-	-	15.02	9.46	1.64	15		
			*	II	11.39	10.98	11.00	15.02	8.18	1.76	16		
			**	I	11.43	-	-	15.02	9.46	-	-		
			256	I	11.39	-	-	13.23	9.46	1.36	7		
			128	I	11.07	-	-	13.28	9.88	1.31	6		
			58	I	14.39	-	-	15.02	13.76	1.11	2		

*Unweighted average of all measurements in this mode.

**Average weighted by total integration time.

TABLE X. — COMPARISON OF BRIGHTNESS TEMPERATURES MEASURED BY
S193 WITH ACCEPTED AND OR GROUND TRUTH VALUES FOR SL3

TASK SITE NAME AND NUMBER TIME	MODE	POL	ANGLE OF INCI- DENCE	ANALYSIS TECHNIQUE	MEASURED BRIGHTNESS TEMPERATURE (S193) °K						NUMBER OF SAMPLES	ACCEPTED/GROUND TRUTH BRIGHTNESS TEMPERATURE	
					Mean	Median	Mode	Max	Min	Std Dev		Brightness Temp °K	Source
Gulf of Mexico 749598 Pass 13 Start 216:17:26:45 Stop 216:17:26:59	CTC R/S	H*	0-4 4-8 8-12	0/II 0/II 0/II	130.60 131.50 132.83	130.66 131.46 132.57	130.17 131.50 132.50	133.14 133.75 136.18	126.51 128.66 130.38	1.82 1.33 1.50	10 14 14	125±5 126±5 127±5	Paris (2,3,4)
Gulf of Mexico 749598 Pass 13 Start 216:17:27:01 Stop 216:17:29:49	CTC R/S	V*	0-4	0 II	135.15 134.85	134.83 134.80	134.92 134.92	173.05 142.85	131.26 131.26	3.45 1.32	308 305	125±5	Paris (2,3,4)
			4-8	0 II	134.47 134.40	134.40 134.39	134.32 134.32	153.04 138.02	130.47 130.47	1.73 1.37	356 354	124±5	
			8-12	0 II	134.28 134.30	134.31 134.32	134.16 134.16	137.97 137.97	129.45 130.73	1.40 1.36	229 228	123±5	
Gulf of Mexico 749598 Pass 13 Start 216:17:25:18 Stop 216:17:26:21	CTC R/S	H*	0-4	0 I II	133.53 132.46	131.73 131.71	131.82 131.82	164.95 149.63	128.18 128.18	6.31 3.28	102 96 98	125±5	Paris (2,3,4.
			4-8	0 I II	133.75 132.97	132.44 132.39	132.03 132.03	166.83 145.58	127.19 127.19	4.94 2.84	121 113 116	126±5	
Gulf of Mexico 749598 Pass 16 Start:220:16:5:39 Stop :220:16:7:20	ITNC R/S	V	44-55	0 II	169.20 167.67	167.22 167.10	166.13 166.13	187.52 174.78	165.61 165.61	6.16 2.65	13 12	175±5	Paris (2,3,4
			36-44 27-33	0/II 0/II	156.75 143.37	156.27 143.18	156.05 143.50	159.54 145.84	155.53 141.32	1.38 1.34	12 10	156±5 140±5	
			13-18 0-3	0/II 0/II	132.50 130.59	132.12 130.86	132.17 131.50	134.09 132.04	131.52 128.61	0.98 1.60	7 4	129±5 125±5	

*Polarization is defined in terms of the sensor's selected input port. For crosstrack modes, this does not correspond to the polarization incident at the target.

TABLE X. — COMPARISON OF BRIGHTNESS TEMPERATURES MEASURED BY
S193 WITH ACCEPTED AND/OR GROUND TRUTH VALUES FOR SL3 (CONCLUDED)

TASK SITE NAME AND NUMBER TIME	MODE	POL	ANGLE OF INCIDENCE	ANALYSIS TECHNIQUE	MEASURED BRIGHTNESS TEMPERATURE (S193) °K						NUMBER OF SAMPLES	ACCEPTED/GROUND TRUTH BRIGHTNESS TEMPERATURE	
					Mean	Median	Mode	Max	Min	Std Dev		Brightness Temp °K	Source
Gulf of Mexico 749598 Pass 20	ITC	V.	44-55	0	164.50	164.42	164.39	174.38	159.53	2.37	144	175±8	Paris (2,3,4)
				II	164.23	164.35	164.39	169.74	159.53	1.78	140		
			36-44	0	155.72	155.59	154.44	166.22	149.01	3.27	208	156±5	
				II	155.57	155.47	154.44	163.30	149.01	3.05	205		
Start:224:14:49:20 Stop :224:14:51:50			28-36	0	147.18	146.86	143.16	158.69	140.86	3.39	146	140±5	
				II	146.95	146.75	143.16	152.70	140.86	3.10	142		
			8-16	0	135.61	135.39	134.64	141.88	130.82	1.96	267	128±5	
				II	135.54	135.36	134.64	139.74	130.82	1.87	264		
			0-8	0	134.72	134.64	134.38	140.71	129.98	1.96	297	125±5	
				II	134.70	134.63	134.38	139.83	129.98	1.94	296		

computed by Paris's model are considered to be lower bound values since brightness temperatures rise as the ocean roughness increases. Note that some of the Pass 13 results appear to be biased upward by heavy clouds and precipitation.

7.3.3 <u>Great Salt Lake Desert Results from SL3</u>. Before the Skylab missions, the Great Salt Lake Desert was selected as a constant temperature hot target for sensor performance evaluation. However, the data from S193 demonstrates the Great Salt Lake Desert is not a constant temperature target. This is vividly demonstrated in table XI where S193 measurements have been summarized. Notice that a brightness temperature range of over 60°K is encountered.

Further confirmation that the Great Salt Lake Desert is a non-uniform temperature target is given in figure 10, which is a plot of the X-band Airborne Multifrequency Microwave Radiometer data (10.625 GHz) gathered over the test sites.

Results from a pass near the Great Salt Lake Desert, but not over it, are also shown in table XI. The brightness temperatures measured by S193 were about 7°K higher than comparable S194 measurements. This is reasonable for a land target.

7.3.4 <u>Sahara Desert Results from SL3</u>. The Sahara Desert proved to be one of the most uniform high temperature targets viewed by the S193 Radiometer. The brightness temperatures measured by S193 were 3° to 7° higher than comparable S194 measurements as shown in table XI. This is a reasonable difference to expect for land targets at the two instrument's frequencies.

MFMR MISSION 253 FLT 11 SITE 116 PROJ S194 FLT DATE 08/10/73
CORRECTED X BAND ANTENNA TEMPERATURE

DEGREE K

300
250
200
150
100
50
0
-50
-100

022 39 35 022 40 25 022.41:15 022.42.05 022·42 55 022 43·45 022 44.35 022 45 25 022 46 15 022 47 05 022.47·55 022 48 45 022.49.35 022.50·25 022 51.15 022 52.05 022 52.55 022.53·45 022 54 15
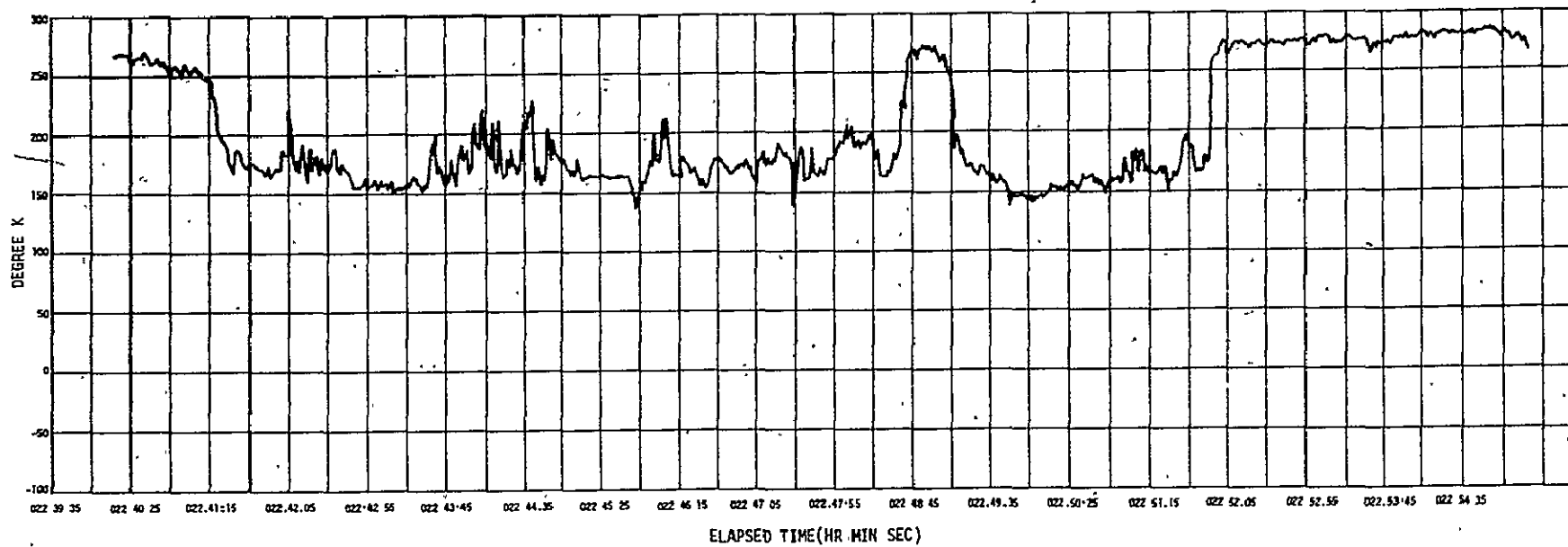
ELAPSED TIME(HR MIN SEC)

Figure 10. — Xband MFMR measurements over Great Salt Lake desert.

TABLE XI. — COMPARISON OF BRIGHTNESS TEMPERATURES MEASURED BY
S193 WITH ACCEPTED VALUES AND S194 MEASUREMENTS FOR SL3

TASK SITE NAME AND NUMBER TIME	MODE	POL	ANGLE OF INCIDENCE (DAY)	ANALYSIS TECHNIQUE	MEASURED BRIGHTNESS TEMPERATURE (S193) °K						NUMBER OF SAMPLES	S194 BRIGHTNESS TEMPERATURE	
					Mean	Median	Mode	Max	Min	Std Dev		Brightness Temperature	Source
Near Great Salt Lake Desert Utah 749233 Pass 12 Start: 215:18:01:31 Stop : 215:18:02:13	CTC R/S Pitch 0° Roll 30° Left	H*	22-35	0	277.30	277.50	277.71	283.93	268.80	2.38	241	μ=270.4 σ= 2.4 Min=265.7 Max=275.0 126 Samples	S194 Data From Pass 12 (15)
				II	277.37	277.50	277.71	283.93	270.70	2.28	239		
Great Salt Lake Desert 749 233 Pass 16 Start: 16:00:54 Stop : 16:01:05	CTC R/S Pitch 15°	V*	16-20	0	222.62	217.01	208.17	261.11	199.41	17.85	24	μ=270.1 σ= 1.7 Max=274.1 Min=262.9 249 Samples	S194 Data From Pass 16 (15)
				II	220.95	215.48	208.17	250.68	199.41	16.17	23·		
Sahara Desert Pass 21 Start: 15:36:06 Stop : 15:36:51	CTC R/S	H*	0-4	0	285.11	285.05	285.85	290.79	277.35	2.39	87	μ=281.5 σ= 1.8 Max=284.6 Min=278.1 297 Samples	S194 Data From Pass 21 (15)
				II	285.20	285.06	285.85	290.79	279.17	2.25	86		
			4-8	0	284.75	284.83	285.88	289.92	277.91	2.28	106		
				II	284.82	285.01	285.88	289.92	279.60	2.19	105		
			8-12	0	284.94	285.12	285.36	291.11	274.84	2.76	62		
				II	285.10	285.14	285.36	291.11	277.15	2.46	61		
Sahara Desert Pass 21 Start: 15:36:53 Stop: 15:37:07	CTC R/S	V*	0-4	0/II	282.01	282.19	281.30	285.49	278.88	1.76	12		
			4-8	0/II	281.59	282.10	283.50	284.46	276.79	2.13	15		
			8-12	0/II	281.16	281.24	280.50	284.46	278.26	1.82	11		

*Polarization is defined in terms of the sensor's selected input port. For crosstrack modes, this does not correspond to the polarization incident at the target.

TABLE XI. — COMPARISON OF BRIGHTNESS TEMPERATURES MEASURED BY
S193 WITH ACCEPTED VALUES AND S194 MEASUREMENTS FOR SL3 (CONCLUDED)

TASK SITE NAME AND NUMBER TIME	MODE	POL	ANGLE OF INCI-DENCE (DAY)	ANALYSIS TECHNIQUES	MEASURED BRIGHTNESS TEMPERATURE (S193) °K						NUMBER OF SAMPLES	S194 BRIGHTNESS TEMPERATURE	
					Mean	Median	Mode	Max	Min	Std Dev		Brightness Temperature	Sourc
Sahara Desert Pass 22 Start 14:52:40 Stop : 14:52:57	CTC R/S	H*	0-4	0/II	286.25	286.29	286.50	291.15	281.98	2.42	32	μ=279.4 σ= 3.2 Max=283.1 Min=274.8 495 Samples	S194 Data From Pass. 22 (15)
			4-8	0/II	286.40	286.45	286.88	290.30	282.35	1.95	40		
			8-12	0/II	287.59	287.27	286.50	292.69	283.82	2.34	24		
Sahara Desert Pass 22 Start 14:52:14 Stop : 14:52:40	CTC R/S	V*	0-4	0/II	282.48	282.93	283.07	286.00	278.22	2.09	33		
			4-8	0/II	282.42	282.54	282.93	289.04	276.90	3.01	41		
			8-12	0/II	281.92	282.08	282.83	286.44	276.47	2.83	26		

7-33

7.3.5 <u>Other Land Target Results from SL3</u>. In order
to partially overcome the failure of the Great Salt Lake
Desert as a constant temperature site, a number of S193
data-takes during SL3 were examined. Those which show the
characteristics of constant temperature targets are pre-
sented in table XII. No ground truth information was avail-
able for these sites.

7.4 Deep Space Results From SL4

During the entire SL4 mission, the S193 antenna pattern
was degraded. The antenna main beam accounted for only
about 1/6 to 1/12 of the total power received. The major
portion of power received came from a very broad beam with
the antenna responding to targets as much as 72° from bore-
sight. Under these conditions, only deep space of all
observed targets could qualify as a constant temperature
target. To have included other targets from the SL4 mis-
sion in a profitable manner would have required far more
extensive effort than could be justified by the resources
available. The SL4 deep space results provide significant
data in determining the long-term stability of the instrument.

The S193 Radiometer measurements from SL4 have been
summarized in tables XIII and XIV.

The underlined data represents the author's profes-
sional judgment of which analysis method has provided results
that are most representative of actual sensor performance
without overstating the instruments precision and accuracy.

TABLE XII. — BRIGHTNESS TEMPERATURES MEASURED BY S193 FOR SL3

TASK SITE NAME AND NUMBER TIME	MODE	POL	ANGLE OF INCIDENCE (DEG)	Analysis Technique	MEASURED BRIGHTNESS TEMPERATURE (S193) °K						NUMBER OF SAMPLES	ACCEPTED/GROUND TRUTH BRIGHTNESS TEMPERATURE	
					Mean	Median	Mode	Max	Min	Std Dev		Brightness Temp °K	Source
Kansas, Oklahoma Pass 15 Start:16:37:40 Stop :16:38:20	CTC R/S Pitch 30°	V	32-36	0	279.44	280.64	280.67	288.03	253.03	5.88	225	-	NONE
				I	280.64	-	-	288.03	≈268.00	3.25	212		
				II	280.34	280.84	280.67	288.03	263.17	3.87	216		
Texas Pass 16 Start:16:03:58 Stop 16:04:42	CTC R/S Pitch 30°	V	28-32	0	284.20	284.50	284.41	288.30	273.76	2.34	130	-	NONE
				I	284.42	-	284.41	288.30	≈278.00	1.89	127		
				II	284.36	284.53	284.41	288.30	277.24	1.99	128		
			32-36	0	283.00	283.61	283.86	287.99	265.12	3.43	88		
				II	283.49	283.66	283.86	287.99	278.10	2.19	85		
Indiana, Ohio Pass 17 Start:13:45:17 Stop :13:45:38	INC R/S	H	ALL	0	267.85	268.67	268.90	269.36	264.18	2.13	6	-	NONE
		V	ALL	0	269.44	268.99	-	272.11	267.38	2.09	6	··	
New Mexico, Texas Pass 20 Start:14:46:28 Stop :14:47:22	CTC R/S Roll 15° Left	V	8-12	0/II	272.80	272.73	272.83	277.14	268.77	2.03	41	-	NONE
			12-16	0/II	272.95	273.18	273.90	277.13	269.21	2.02	44		
			16-20	0/II	273.29	273.17	273.75	278.00	269.21	2.06	42		
			20-24	0	273.22	274.05	274.36	277.13	260.41	3.17	34		
				I	273.84	-	-	277.13	≈269.50	1.79	32		
				II	273.60	274.05	274.36	277.13	266.13	2.24	33		
			24-28	0/II	273.15	273.62	274.07	276.26	269.21	2.08	17		

TABLE XIII. — COMPARISON OF BRIGHTNESS TEMPERATURES MEASURED BY
S193 WITH ACCEPTED VALUES AND S194 MEASUREMENTS FOR SL4

TASK SITE NAME AND NUMBER TIME	MODE	POL	IT (MSEC)	ANALYSIS TECHNIQUE	MEASURED BRIGHTNESS TEMPERATURE (S193) °K						NUMBER OF SAMPLES	ACCEPTED/S194 BRIGHTNESS TEMPERATURES	
					Mean	Median	Mode	Max	Min	Std Dev		Brightness Temp.°K	Source
Deep Space 749007 LC-4 Pass 63 Start:343:00.26:01 Stop :343:00:26.21	CTC R/S	H	32	0 I II	6.74	-	-	10.40	3.81	1.18	110	2.8° ±0.5° Uncertainty	Literature (6,7)
Deep Space 749007 LC-4 Pass 63 Start:343:00:23:37 Stop :343:00:26 01	CTC R/S	V	32	0 I II	8.95 8.97	9.09 9.10	9.25 9.25	12.99 12.99	3.30 4.09	1.65 1.61	814 810	μ=3.4 σ=0.3 Max=3.8 Min=3.0 2889 Samples	S194 Data From SL-4 LC-4
Deep Space 749007 LC-4 Pass 63 Start:343:00:17:12 Stop :343:00:23:04	CTC RAD ONLY	H	58	0 I II	12.74 12.69	12.39 12.36	10.76 10.76	19.56 18.73	6.62 6.62	2.66 2.61	1957 1942		
		V	58	0 I II	12.02 12.02	11.80 11.80	10.43 10.43	18.71 18.41	6.17 6.17	2.67 2.66	1955 1953		
Deep Space Pass 63 LC-4 Start:343:00:30:59 Stop :343:00:33.43	CTNC R/S	H	* * *	0 I II	8.13 8.78 8.13	9.22 - 9.22	10.64 10.64 10.64	12.94 12.94 12.94	- 0-26 -	3.71 3.09 3.71	54 50 54		
		V	* * *	0 I II	6.96 7.98 6.96	8.37 - 8.37	9.88 9.88 9.88	11.80 11.80 11.80	- 0.29 -	3.59 2.54 3.59	55 48 55		

7-37

TABLE XIV. — COMPARISON OF BRIGHTNESS TEMPERATURES MEASURED BY
S193 WITH ACCEPTED VALUES AND S194 VALUES FOR SL4

TASK SITE NAME AND NUMBER TIME	MODE	POL	IT (MSEC)	ANALYSIS TECHNIQUE	MEASURED BRIGHTNESS TEMPERATURE (S193) °K						NUMBER OF SAMPLES	ACCEPTED/S194 BRIGHTNESS TEMPERATURES	
					Mean	Median	Mode	Max	Min	Std Dev		Brightness Temp °K	Source
Deep Space 749007 Pass 75 (LC-V) Start:13:09:02 Stop :13:11:31	CTC R/S	H	32	0 II	10.55 10.15	10.13 10.13	10.67 10.67	349.98 18.92	6.21 6.21	11.78 1.25	842 841	2.8° ±0.5° Uncertainty	Literature (6,7)
Deep Space 749007 Pass 75 (LC-V) Start:13:06:37 Stop :13:09:01	CTC R/S	V	32	0 II	7.80 7.82	7.81 7.82	7.87 7.87	11.99 11.06	2.67 3.93	1.29 1.23	816 809	μ=3.1 σ=0.3 Max=3.5 Min=2.6 2886 Samples	S194 Data From SL-4 LC-5
Deep Space 749007 Pass 75 (LC-V) Start:13:00:08 Stop :13:00:05	CTC RAD ONLY	H	58	0 II	16.09 16.08	15.97 15.97	15.94 15.94	20.69 19.87	11.70 12.11	1.41 1.40	1983 1977		
		V	58	0 II	14.80 14.78	14.74 14.74	14.57 14.57	20.66 18.84	10.52 10.52	1.50 1.47	1981 1974		
Deep Space 749007 Pass 75 (LC-V) Start:13:13:56 Stop :13:16:47	CTNC R/S	H	* * *	0 I II	10.73 9.61 10.73	9.88 - 9.88	9.79 9.79 9.79	23.05 19.28 23.05	0.19 0.19 0.19	5.37 4.22 5.37	56 51 56		
		V	* * *	0 I II	9.16 9.67 9.16	8.76 - 8.76	9.00 9.00 9.00	18.85 18.85 18.85	0.00 ≈1.00 0.00	4.59 4.18 4.59	56 53 56		

*Unweighted average of all measurements in this mode.

This judgment is based upon consistency of results, antici-
pated performance of the sensor, and knowledge of charac-
teristics of the target.

8.0 PRECISION

The form of the precision and accuracy estimates has been guided in general by the recommendations of Eisenhart[16] and Ku[17] of the National Bureau of Standards. However, the following modifications have been made to partially compensate for the varying number of samples and for convenience of investigation. An unbiased estimate of standard deviation has been substituted for S. In addition, estimates of standard deviation have been quoted to three significant figures instead of two significant figures.

Two interpretations of precision have been given. The first interpretation of precision is the repeatability of measurements of an assumed constant temperature target during a single time slice of data. In practice, this interpretation of precision relies on unbiased estimates of the standard deviation of brightness temperature measurements over an assumed constant temperature target. This quantitatively will be reported as short-term precision in section 8.1.[2]

The second interpretation of precision is a comparison between means of measurements taken of an assumed constant temperature target during two or more different time slices of data, preferably taken during different Skylab passes. This will be reported in a more qualitative manner as long-

---

[2]For a theoretical evaluation of radiometer receiver sensitivity and resolution and additional experimental data, see section 8 in Skylab Program Earth Resources Experiment Package Final Report, Sensor Performance Report S193 Rad Scat, TR236-4, prepared by the University of Kansas, Center for Research, Inc., Lawrence, Kansas, July 15, 1975.

term precision in section 8:2 since the differences which appear may be in part caused by changes in the target from day-to-day or season-to-season.

Originally, separate evaluations of precision for SL2 and SL3 had been planned. However, as, the data was examined, no significant long-term trends were discernable during SL2 and SL3 and the total data base for evaluation was limited. Therefore, it has been assumed that the precision was the same for both missions.

8.1 Short-Term Precision

The unbiased estimate standard deviation of measurements during a single time slice over a "constant temperature" target was taken as the measure of short-term precision. Since there is some brightness temperature variance in even the chosen constant temperature targets, the minimum standard deviation, for which more than 10 to 15 measurements were taken in a given target temperature range, is chosen as the correct value. In a few cases where there were 15 or fewer measurements, unbelievably low standard deviations occurred. These have been plotted on the graphs but are ignored in the analysis of precision and accuracy.

In some temperature ranges for some modes, data is either absent or unreasonable. To fill in these gaps the following procedure was followed. First, following generally accepted theory in calculating a radiometer's sensitivity, the sensitivity was assumed to be proportional to system temperature[18] where

$$T_{SYS} = T_{RN} + T_B \qquad (27)$$

T_{SYS} = System temperature °K.

T_{RN} = Receiver noise temperature °K = 1200.

T_B = Measured brightness temperature of the target as seen by the antenna °K.

An additional 20 percent was added to cover factors which may degrade the radiometer's performance from values obtained by linear scaling. Summarizing this in equation form:

$$\sigma_{TU} = 1.2 \left(\frac{T_{RN} + T_U}{T_{RN} + T_M} \right) \sigma_{TM} \qquad (28)$$

where

σ_{TU} = Predicted standard deviation (precision) at target temperature T_U (in °K).

σ_{TM} = Measured standard deviation (precision) at target temperature T_M (in °K).

T_M = Target temperature at which precision is measured (in °K).

T_U = Target temperature at which precision must be estimated (in °K).

Scaling is done from the measured value at the closest target temperature to minimize any errors that result from extrapolation. The results of this analysis appear in figures 11 through 15.

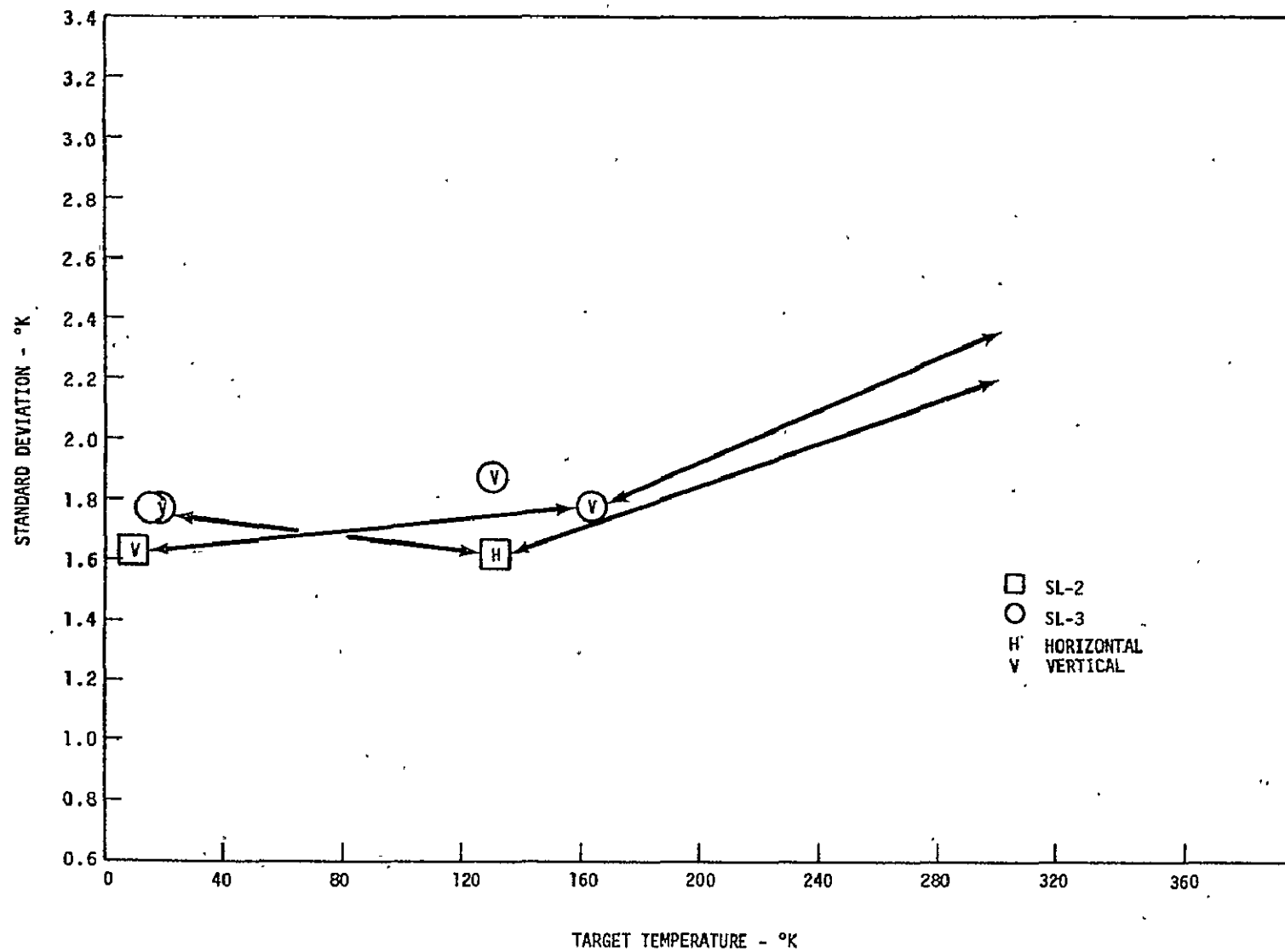Figure 11. — S193 Radiometer precision for ITC R/S mode.

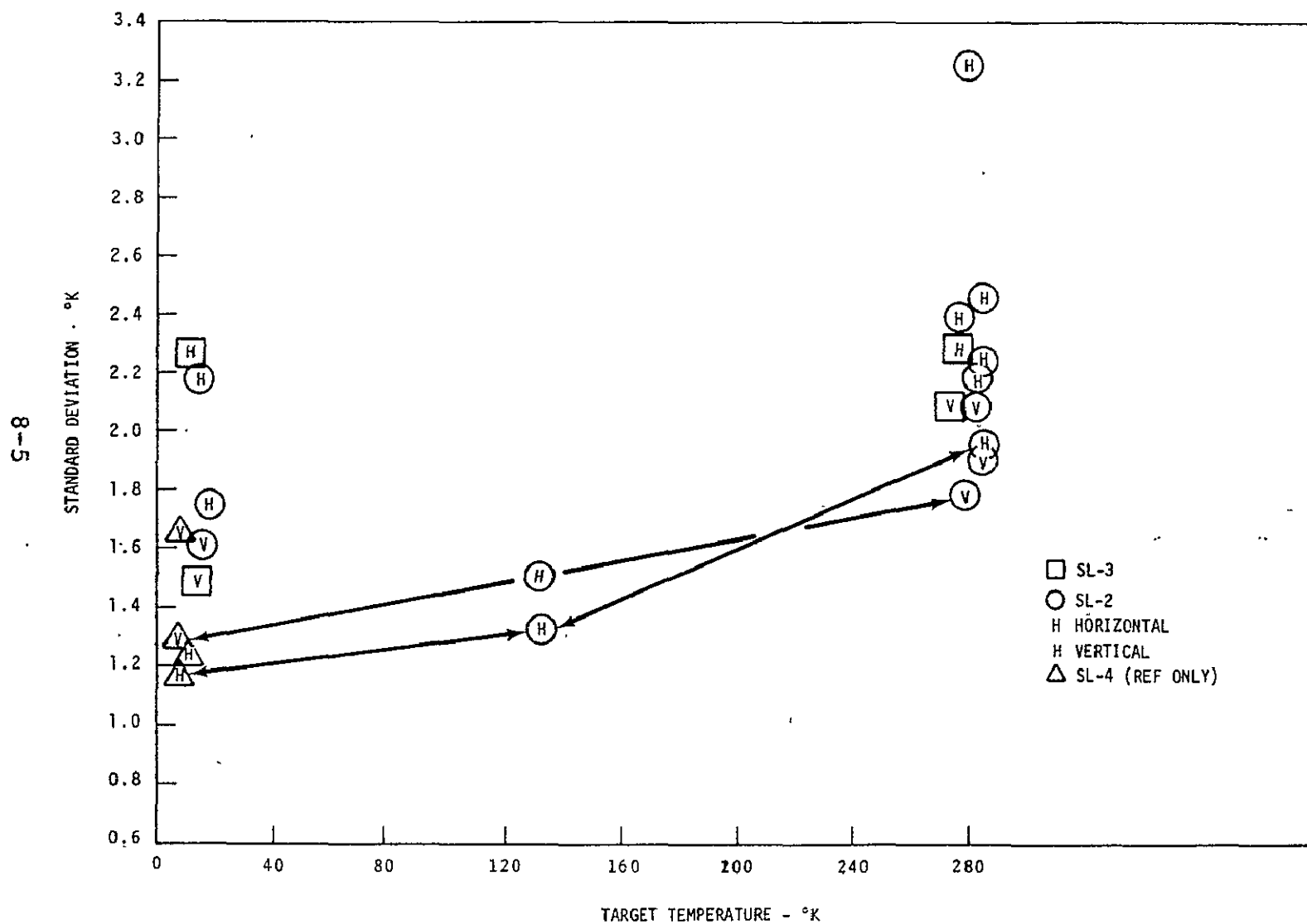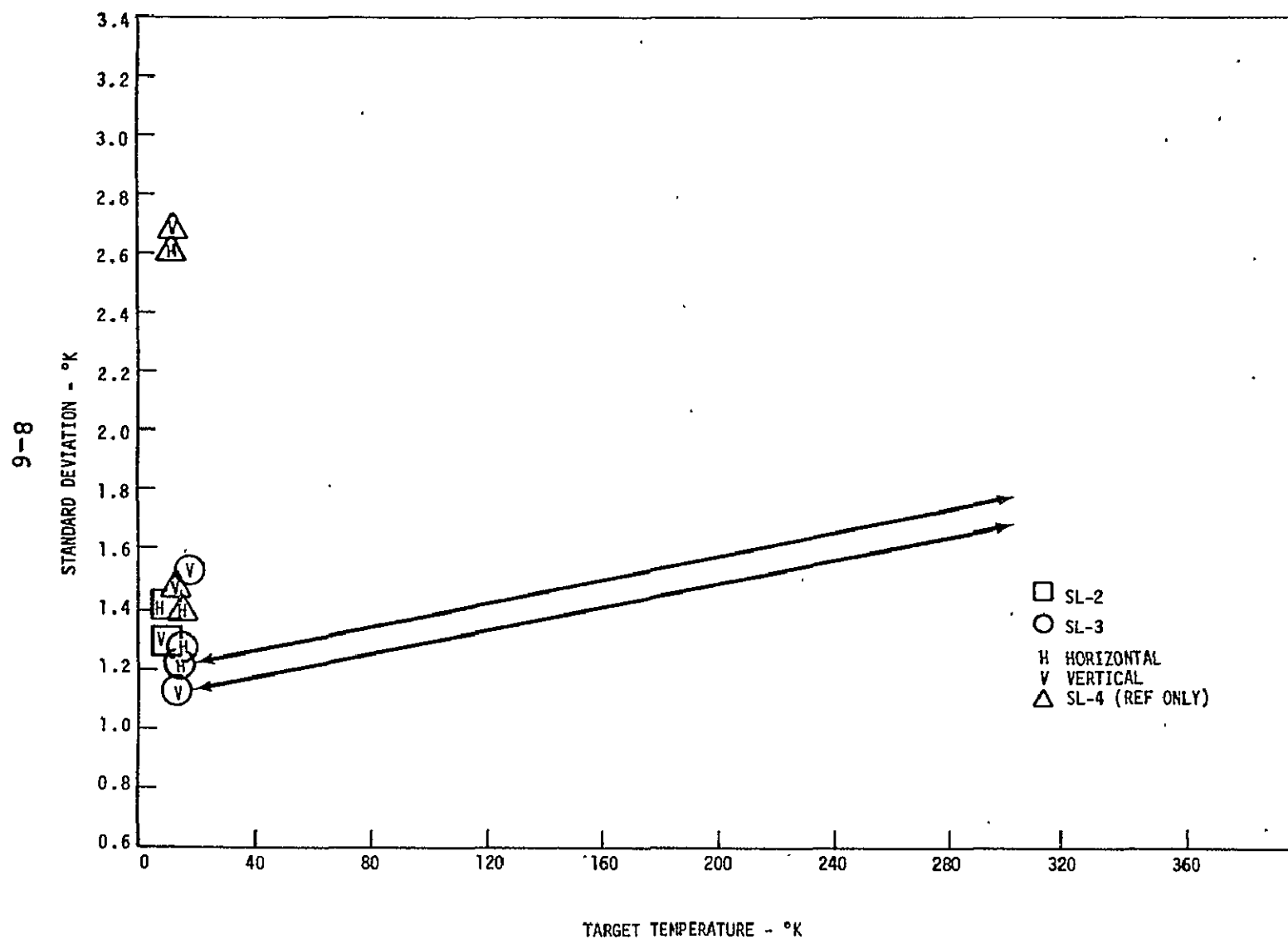Figure 12. — S193 Radiometer precision for CTC R/S mode.
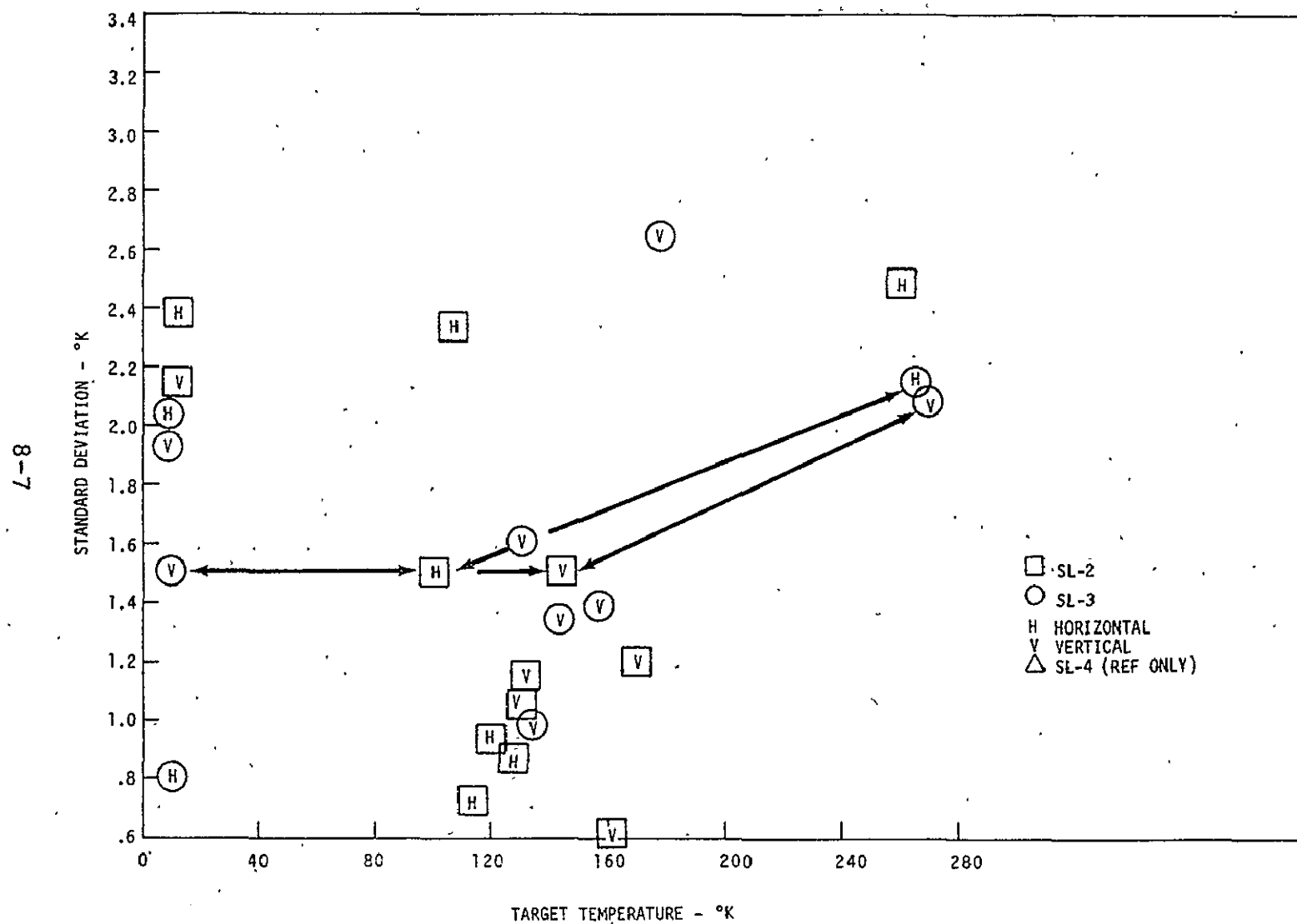
Figure 13. — S193 Radiometer precision for CTC RAD mode.

9-6

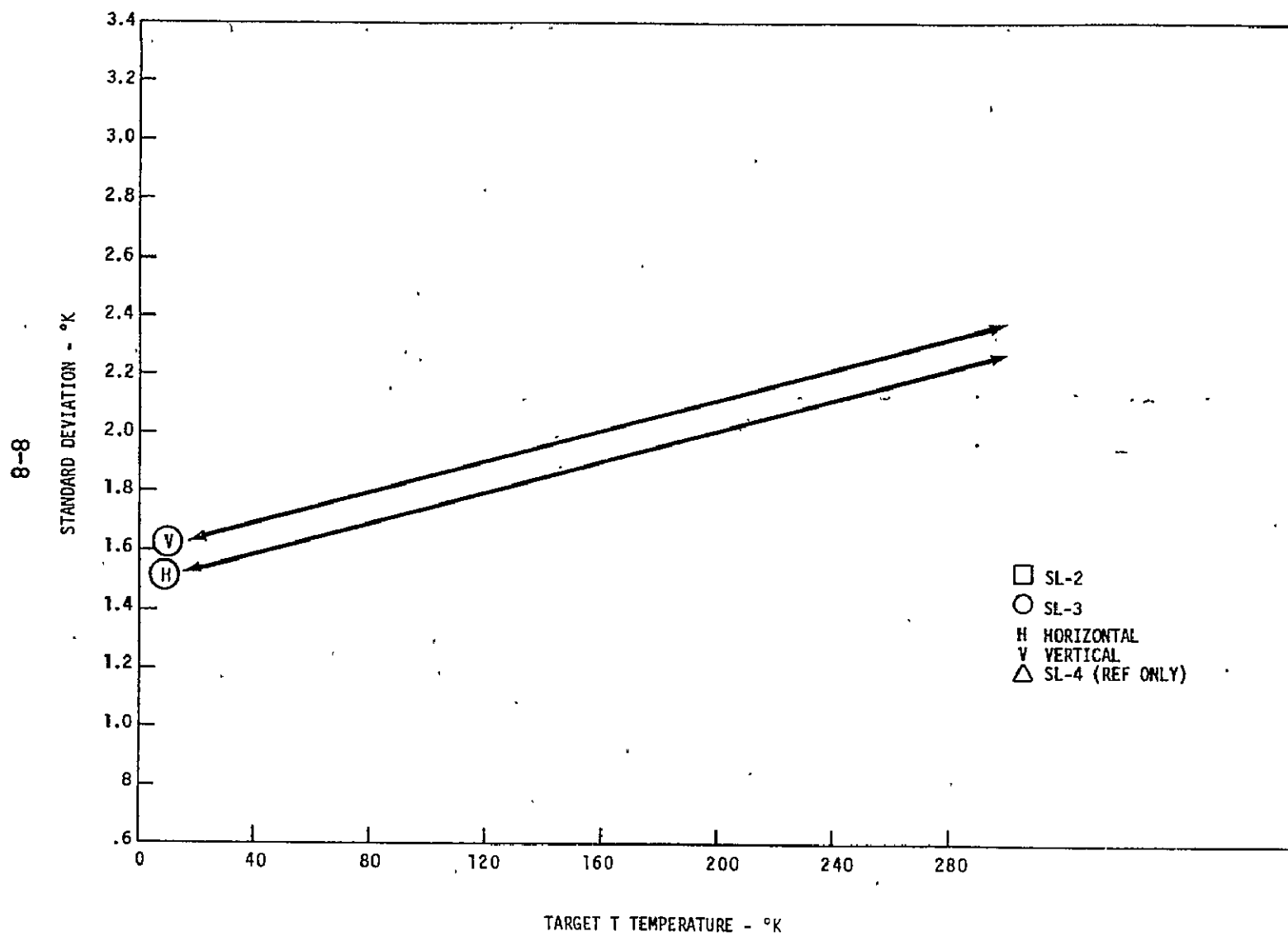Figure 14. — S193 Radiometer precision for ITNC R/S mode.

8-8

Figure 15. — S193 Radiometer precision for CTNC R/S mode.

8.2 Long-Term Precision

Comparisons for time slice to time slice, mission-to-mission, and mode-to-mode have been made for three targets. Table XV gives the comparison for deep space while tables XVI and XVII give results for the Gulf of Mexico at low incidence angles and the Sahara Desert, respectively.

For the deep space passes, repeatability from mode-to-mode, pass-to-pass and mission-to-mission is not particularly good. Differences in means from time-to-time in a single mode and polarization range up to 10.46°K while differences between modes in a single Lunar Cal go as high as 12.72°K. Undoubtedly, a portion of this variation is due to "contamination" of the deep space target by energy from the sun, moon, earth or other warm targets appearing somewhere in the antenna pattern. Obviously, the amount of unwanted energy biasing each result varies from data take to data take.

To note how good repeatability may really be, note that in CTNC R/S Horizontal, the means vary over only 1.25° and the 3σ precision limits for all passes overlap. Consequently, it is reasonable to believe that a significant portion of the variation from time-to-time is in the target or in the case of deep space "contamination of the target" rather than in the instrument. This opinion is further supported by the data from the Gulf of Mexico at low incidence angles. After discarding the data from the time slice which was saturated by the altimeter, the range of mean from maximum to minimum was only 7.68°K. The Gulf of Mexico should have more variation in brightness temperature than deep space since the effects of atmosphere, surface roughness, and foam will be

TABLE XV. — MEAN BRIGHTNESS TEMPERATURES AND 3σ PRECISION
OF MEAN (IN °K) FOR ALL MODES

MODE	POL	LC I DOY165	LC II DOY224	LC III DOY254	LC IV DOY343	LC V DOY17	RANGE	AVERAGE
ITC R/S	V	10.69 ±0.20	17.52 ±0.21	19.57 ±0.21	* -	* -	8.88 -	15.93 -
CTC R/S	H	12.71 ±0.27	17.20 ±0.21	14.18 ±0.36	6.74 ±0.34	10.15 ±0.13	10.46 -	12.20 -
	V	13.09 ±0.17	14.89 ±0.17	14.24 ±0.30	8.95 ±0.17	7.80 ±0.14	7.09 -	11.79 -
CTC RAD	H	13.79 ±0.11	15.79 ±0.10	13.92 ±0.14	12.69 ±0.18	16.08 ±0.09	3.39 -	14.45 -
	V	14.35 ±0.10	16.14 ±0.12	13.87 ±0.13	12.02 ±0.18	14.78 ±0.10	4.12 -	14.23 -
ITNC R/S	H	12.79 ±1.84	10.05 ±0.60	7.49 ±1.33	* -	* -	5.30 -	10.11 -
	V	12.79 ±1.71	10.66 ±1.16	6.85 ±1.25	* -	* -	5.94 -	10.10 -
CTNC R/S	H	10.03 ±0.75	9.62 ±0.89	9.97 ±1.19	8.78 ±1.27	9.61 ±1.77	1.25 -	9.60 -
	V	12.01 ±0.69	11.68 ±0.78	11.39 ±1.32	7.98 ±1.10	9.67 ±1.72	4.03 -	10.55 -
RANGE	H	3.76	7.58	6.69	5.95	6.47	-	-
	V	3.66	6.86	12.72	4.04	6.98	-	-
TOTAL		4.32	7.90	12.72	5.95	8.28	12.83	-

*Mode not exercised.

8-10.

C 2

TABLE XVI. – MEAN BRIGHTNESS TEMPERATURES AND 3σ PRECISION OF MEAN (IN °K) FOR ALL MODES DURING GULF OF MEXICO PASSES

MODE	POL	ANGLE OF INCI-DENCE (DEG.)	PASS 5 DOY156	PASS 8 DOY	PASS 11 DOY165	PASS 13 DOY216	PASS 16 DOY220	PASS 20 DOY224
ITNC R/S	H	0-3	127.17 ±0.91	130.22 ±6.56	-	-	-	-
	V	0-3	129.31 ±1.11	132.55 ±6.38	-	-	130.59 ±2.40	-
ITC R/S	H	0-8	-	-	133.74 ±0.42	-	-	-
	V	0-5	-	-	204.62* ±2.62	-	-	134.70 ±0.34
CTC R/S	H	0-4	-	-	-	130.60 ±1.73 132.46 ±0.99	-	-
	V	0-4	-	-	-	134.85 ±.23	-	-

*This data was taken immediately following an altimeter data take and is probably not valid. Therefore, it has been omitted from all analysis and averages to follow.

TABLE XVII.— MEAN BRIGHTNESS TEMPERATURE 3σ
PRECISION OF MEAN (IN °K) DURING SAHARA DESERT PASS

MODE	POL	ANGLE OF INCI-DENCE	PASS 21 DOY 244	PASS 22 DOY 245	RANGE
CTC R/S	H	0-4	285.20 ±0.73	286.25 ±1.28	1.05
		4-8	284.82 ±0.64	286.40 ±0.92	1.58
		8-12	285.10 ±0.94	287.59 ±1.43	2.49
	V	0-4	282.01 ±1.52	282.48 ±1.09	0.47
		4-8	281.59 ±1.65	282.42 ±1.41	0.83
		8-12	281.16 ±1.65	281.92 ±1.67	0.76

present. Probably at least half of the variations seen are caused by changes in target characteristics.

Data over the Sahara Desert from consecutive passes show excellent repeatability.

Consequently, it is believed that repeatability from mission-to-mission, mode-to-mode, and time-to-time is excellent for targets above 250°K and remains good down to about 120°K, but may not be good for deep space targets.

The estimation of accuracy becomes difficult for S193 because of the very limited measurements available for comparison. Accuracy is a measure of the difference between a measured value and the actual value of a quantity. It includes the systematic or bias errors plus the precision.[19] Since the data is so limited, the values herein represent largely the professional judgments of the authors.

9.1 Bias Errors

To evaluate the bias errors, we use the measured values for the brightness temperature of deep space. Since some of the S193 measurements of deep space were influenced by warm targets, the unweighted mean of the 3 to 5 measurements from all modes will be taken. Deep space is assumed to have a value of 2.8°K. The uncertainty in this value will not be included in this analysis. The measurement means in table XV give the bias errors computed in table XVIII. Apparently, polarization makes little difference in the bias error. For simplicity, accuracy will be determined by using the larger of the two bias errors for a given mode.

For the Gulf of Mexico data, the differences between the S193 measured brightness temperature and the brightness temperature predicted by Paris's smooth sea model were tabulated. After examination of the tabulated values, it appeared that data at the 48° and 40° angles probably were not well predicted by the model. Following examination of the remainder of the data it appeared likely that systematic or bias errors would not exceed 5°K in ITNC, 8°K in ITC, and 6°K in the CTC modes.

TABLE XVIII. — S193 RADIOMETER BIAS ERRORS FOR DEEP SPACE TEMPERATURE

MODE	POL	BIAS ERROR, °K
ITC	V	13.13
CTCR/S	H	9.40
	V	8.99
CTC RAD	H	11.65
	V	11.43
ITNC	H	7.31
	V	7.30
CTNC	H	6.80
	V	7.75

For targets of 280°K or higher in temperature, calibration is sufficiently good that bias errors should not exceed 3°K in any mode.

9.2, Total Uncertainty

The results in tables XVIII and XIX and the conclusions drawn in section 8.0 on precision have been added to form estimates of total uncertainty. The results are presented in figures 16 through 20 which plot the estimated bias errors, the bias errors plus one standard deviation (from the section on precision), and the bias errors plus three standard deviations.

It should be noted that only a limited amount of data was examined to produce these estimates. If more data were analyzed, undoubtedly these limits could be defined more closely.

These plots also indicate the estimated standard deviation or statistical errors for a single point. Where more than one data point is available, the statistical portion of the error for the mean of n measurements will be one standard deviation of the mean $\frac{\sigma}{\sqrt{n}}$ or $\frac{3\sigma}{\sqrt{n}}$ as the investigator chooses.

Throughout this evaluation, proper operation of the instrument has been assumed. This evaluation cannot be considered valid for data takes immediately following altimeter operation when the radiometer processor was saturated.

TABLE XIX. — DIFFERENCES BETWEEN S193 MEASURED
BRIGHTNESS TEMPERATURE AND PARIS'S
SMOOTH SEA MODEL IN DEGREES KELVIN

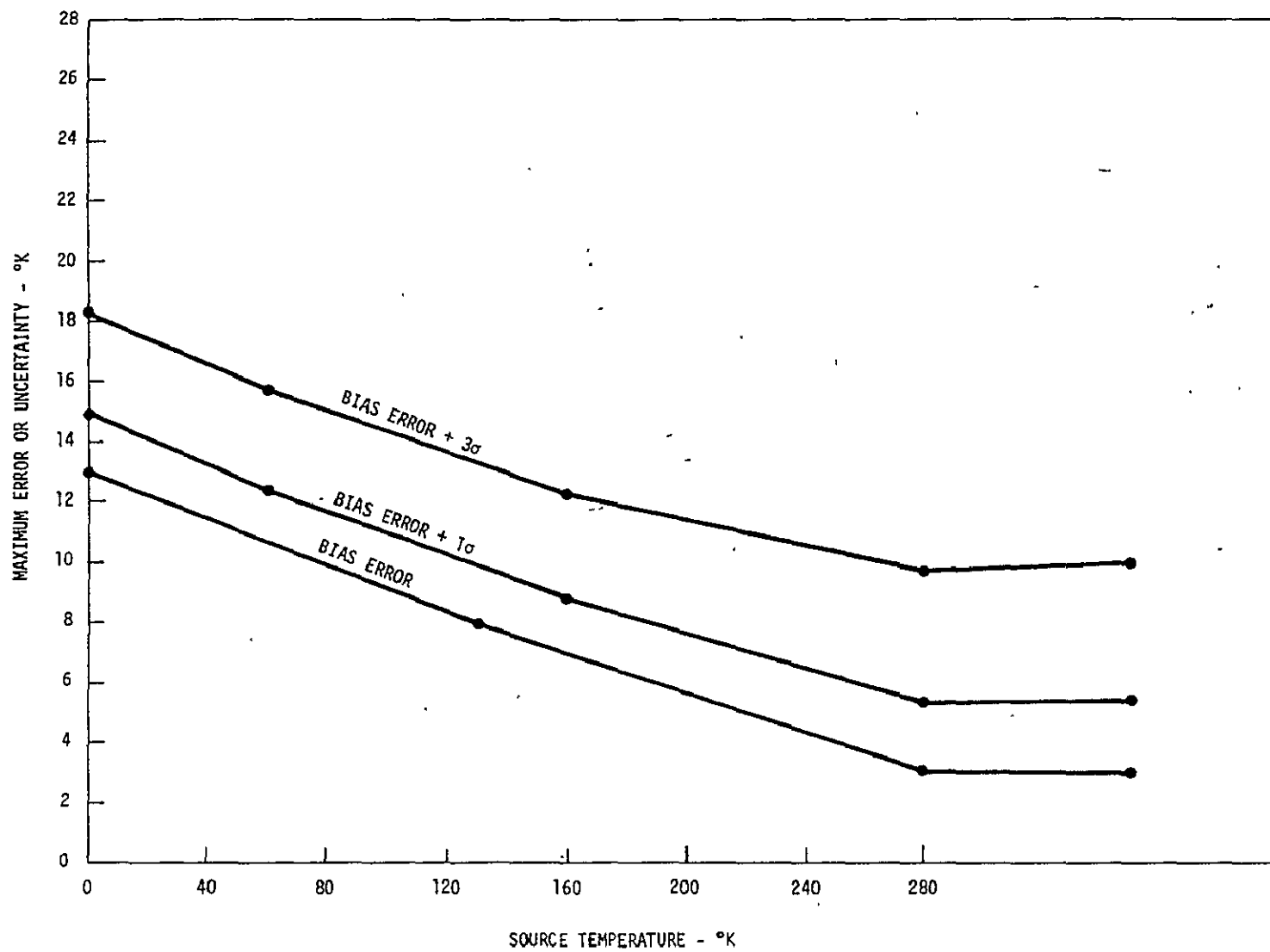| MODE	POL	COMMAND ANGLE	PASS 5	PASS 8	PASS 13	PASS 16	PASS 20
ITNC	H	48°	10.73	18.72	-	-	-
		40	6.65	22.32	-	-	-
		29	4.20	14.48	-	-	-
		15	2.91	7.38	-	-	-
		0	4.17	6.22	-	-	-
	V	48	-4.31	7.08	*	-7.33	*
		40	5.15	7.18	-	0.75	-
		29	4.82	14.05	-	3.37	-
		15	3.83	9.22	-	3.50	-
		0	6.31	8.55	-	5.59	-
ITC	V	48	*	*	*	*	-10.77
		40					-0.53
		29					6.95
		15					7.54
		0					9.70
CTC	H	0-4	*	*	5.60/7.46	*	*
		4-8	-	-	5.50/6.97	-	-
		8-12	-	-	5.83		
	V	0-4	*	*	9.85	*	*
		4-8	-	-	10.40		
		8-12	-	-	11.30		

*Mode not exercised.

Figure 16. — S193 Radiometer estimated accuracy for ITC mode.
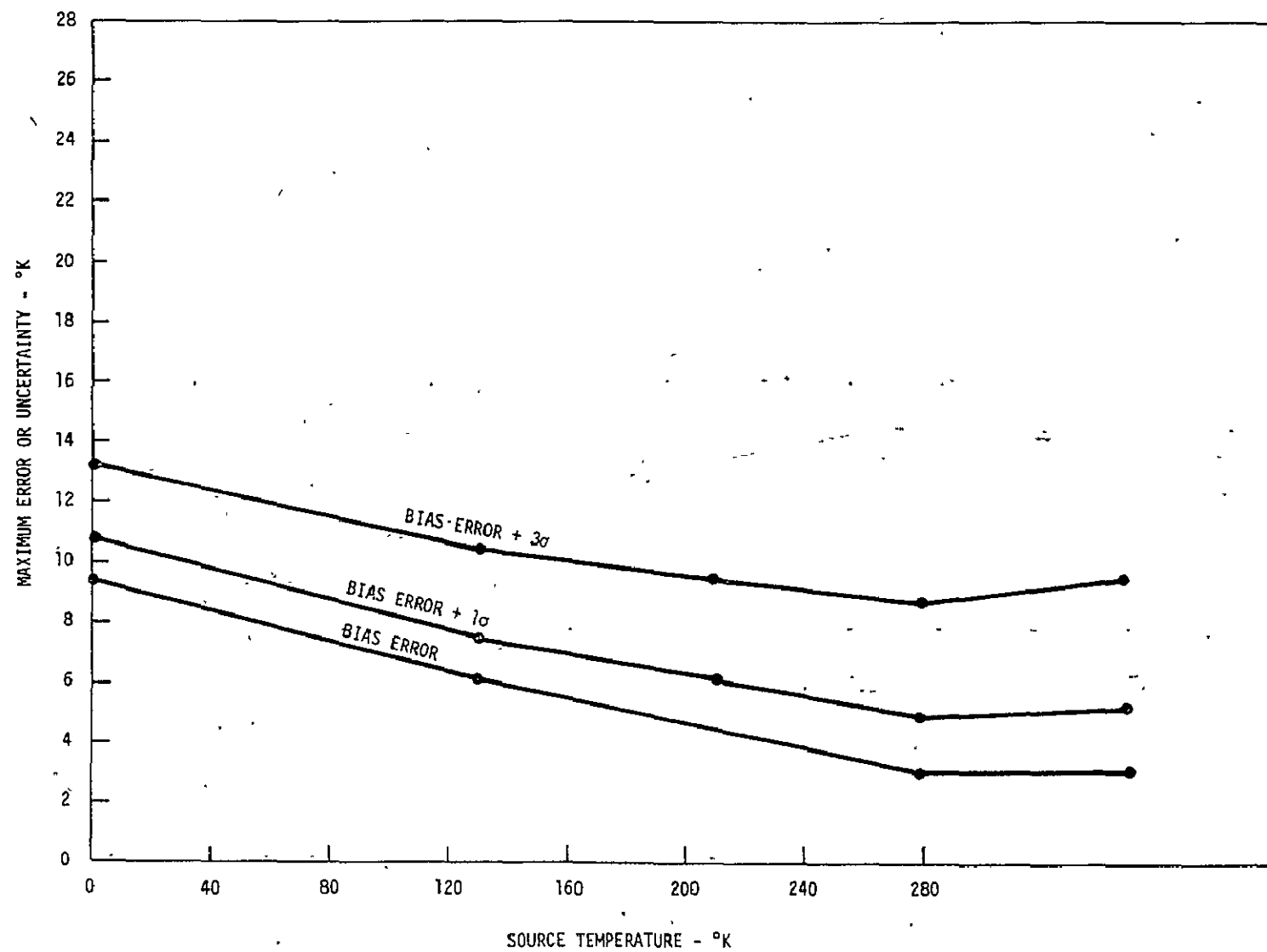
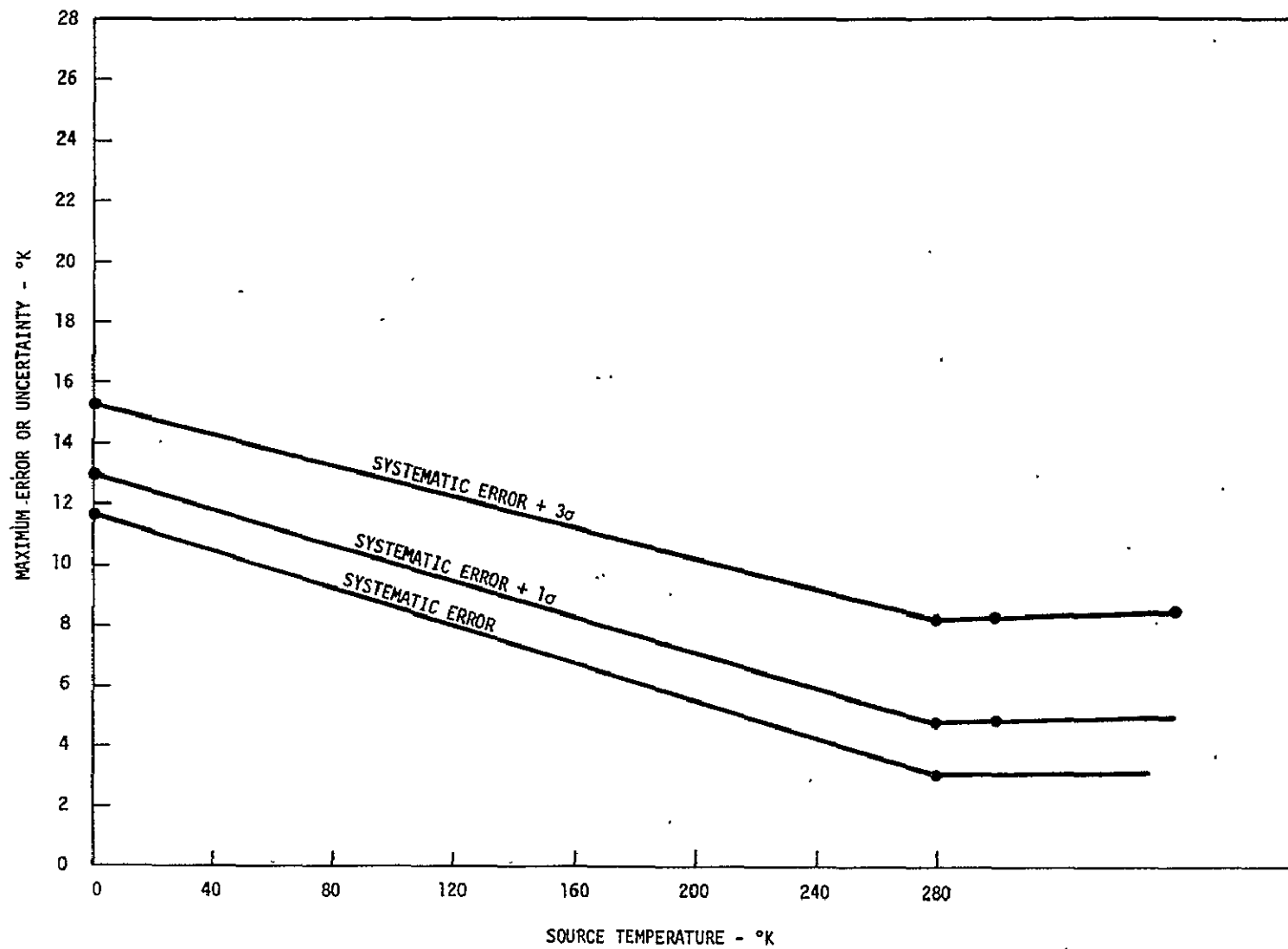Figure 17. — S193 Radiometer estimated accuracy for CTC R/S mode.

Figure 18. — S193 Radiometer estimated accuracy for CTC RAD Mode.
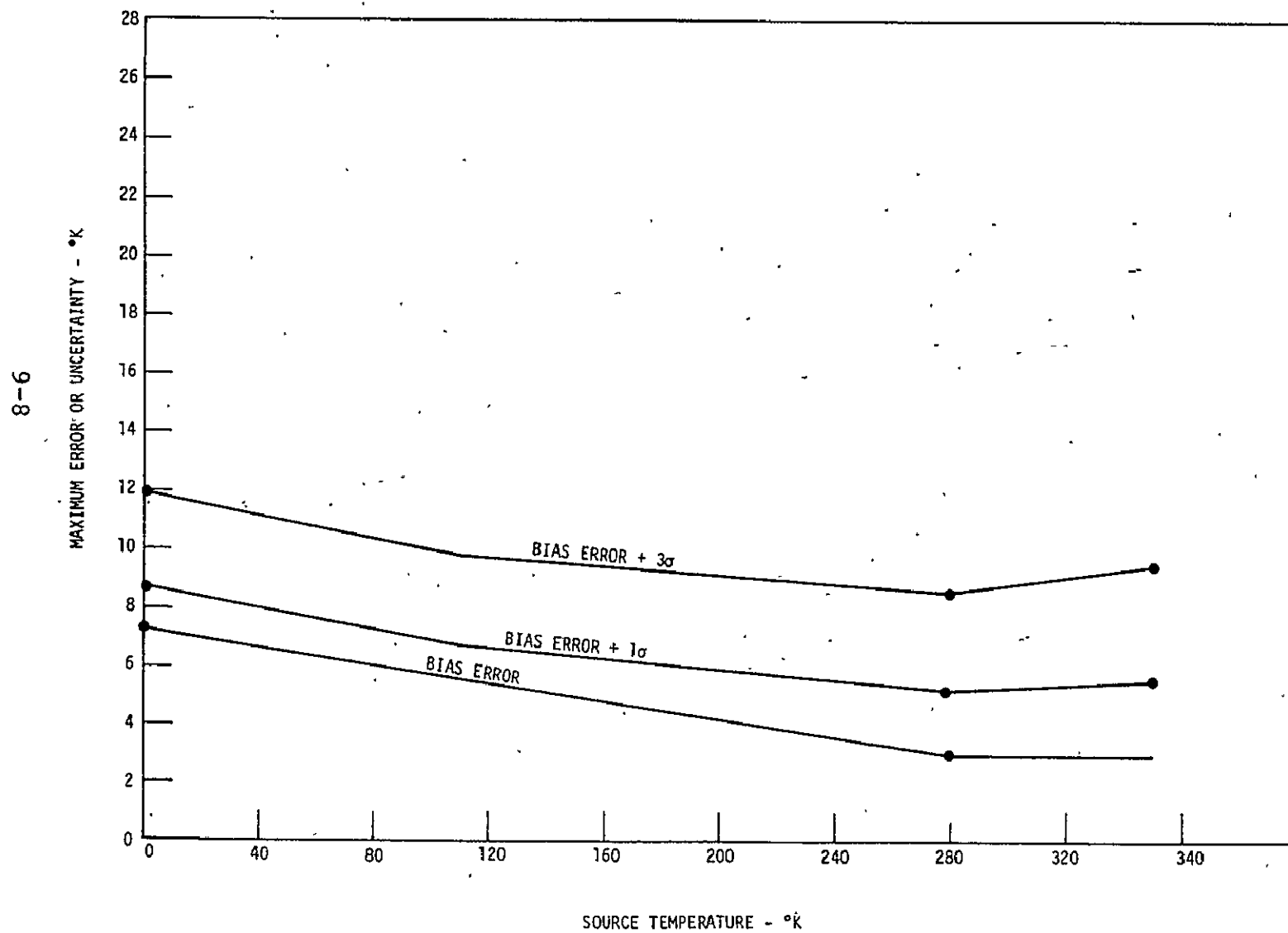
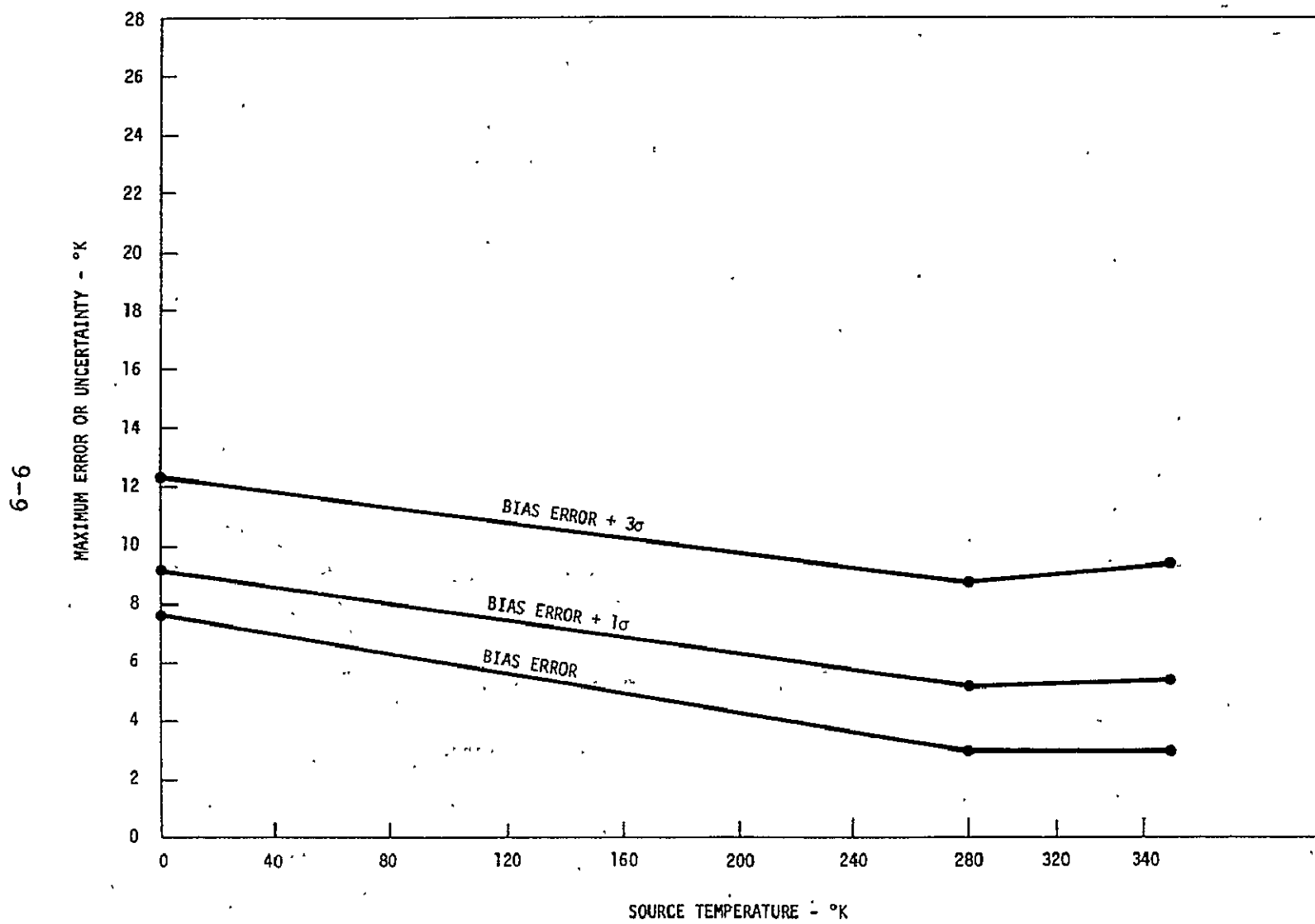Figure 19. — S193 Radiometer estimated accuracy for ITNC mode.

Figure 20. — S193 Radiometer estimated accuracy for CTNC mode.

10.0 ·CONCLUSIONS AND RECOMMENDATIONS

The conclusions and recommendations presented herein cover several general areas. A summary of precision and accuracy achieved by the sensor is given in paragraph 10.1 primarily for the benefit of the principal investigators and others who use the S193 data. Some lessons and recommendations to be gained from experience with S193 in sensor design and operation are presented in 10.2. Data handling and processing recommendations for future sensors are covered in 10.3. Recommendations for future efforts in evaluating sensor performance appear in 10.4.

Finally, some of the significant accomplishments associated with the S193 Radiometer/Scatterometer/Altimeter are presented in 10.5.

10.1 Summary On Performance

The S193 radiometer has performed well as a relative instrument with precisions (1σ) generally being 1.8°K or better in ITC, CTC R/S and CTC RAD-only modes. Precision may have been as high as 2.35°K for ITC on hot (300°K) targets but no data was evaluated there. In the non-contiguous modes, precision was evaluated to be 1.6°K or better for deep space, increasing to 2.2°K or better in ITNC on hot targets. No hot target evaluation for CTNC was possible but precision should be 2.4°K or better there.

At least a portion of the high standard deviations in the non-contiguous modes may really be due to difficulties encountered by the University of Kansas in determining the

K factors (see equation 5 in the appendix) for the three different integration times used in the non-contiguous modes. The amount of data available to the University of Kansas for this evaluation was limited.

When considering the accuracy of S193, it should be noted that the sensor was not specified as an absolute instrument, i.e., no accuracy specification was ever required. The apparently large bias errors present at deep space brightness temperature may also be due to the K factor evaluation. University of Kansas personnel believed that for brightness temperatures below 100°K, the system was non-linear. Considering this assumed non-linearity, the K factors were set to optimize accuracy over the brightness temperature range from about 100°K to 300°K to cover the measurements of terrestrial targets of interest to principal investigators.[20] GE personnel, however, believe that the system is linear down to the coldest targets.[21]

In the absence of adequate comparative measurements, it appears that the bias errors would not exceed 3°K for targets with brightness temperatures of 280°K or more. The bias error is believed to be no more than 6° to 8°K for targets of about 130°K brightness temperature in the contiguous modes and 5 to 6° in the non-contiguous modes. At deep space temperatures (2.8°K) the bias errors are believed to be less than 8°K in the non-contiguous modes and probably do not exceed 9°K to 13.2°K in the contiguous modes. The ITC mode gave the poorest performance, probably because of the very limited calibration time available in that mode.

It is believed that evaluation of more data would lead to a more optimistic evaluation of system performance.

10.2 Sensor Design Conclusions And Recommendations

The rapid advance of microwave and electronics tech-
nology makes it possible to build sensors which will outper-
form S193 and its contemporaries while costing less,
weighing less, requiring less power and being more reliable.
In the next few paragraphs, some of this technology and the
experience gained from S193 are used to generate recommenda-
tions for future sensors.

10.2.1 <u>Antenna gimbals and pointing</u>. The two antenna
gimbal failures, one in pitch during SL3 and one in roll
during SL4, imply that a more reliable antenna scanning
mechanism should be designed for an operational sensor. At
the beginning of the Skylab-4 mission, the astronauts
installed a device on S193 designed by General Electric to
restore operation of the roll gimbal and to pin the pitch
gimbal at zero degrees pitch.

The accuracy of a number of experiments including the
Antenna Pattern Experiment by the University of Kansas was
limited by the pointing accuracy of S193. At least two
factors were involved:

1. The attitude of Skylab was not known to sufficient
   accuracy to pinpoint the center of the antenna
   field-of-view on the ground.

2. The angular readouts of roll and pitch were not
   adequate for determining field-of-view to the
   required accuracy.

In future microwave programs, more attention should be given to the determination of accurate pointing for radiometer and scatterometer systems.

10.2.2 <u>Radiometer integration times</u>. The four different integration times used by the radiometer had different effective gains. This made averaging the calibrations and baselines taken at the different angles in non-contiguous modes difficult. The fact that the data processing had no "look ahead" capability, combined with the instrument's sequence of taking data before the accompanying calibration and baseline, has made data processing in the non-contiguous modes difficult. Some error is undoubtedly introduced by the attempt to normalize and average the calibrations and baselines taken at different antenna angles and through the different integrators which had slightly different gains. However, this error appears to be significantly less than the noise that would be introduced by using only a single calibration.

Consequently, a single radiometer integration time is recommended for future systems. Otherwise, each integration time must be thoroughly characterized.

10.2.3 <u>Polarization</u>. To meet the constraints of Skylab's shroud envelope, the focal length-to-diamater ratio of the S193 antenna was reduced. This factor, plus limitations in the antenna feed and microwave switching network, resulted in low isolation between the vertical and horizontal antenna polarization ports. Based on present estimates of cross-coupling from the University of Kansas, the ratio of power received in desired polarization to power received in

the undesired polarization for the radiometer was only approximately 10 to 13 dB.

An attempt to make a first order correction for this mixing of energy from two polarizations is performed in production data processing. Exact correction is more difficult.

10.2.4 <u>Antenna Feed Design</u>. Photographic evidence indicated that the antenna cap was present during SL4 rendezvous but absent during SL4 undocking. Data analysis indicates that the cap was absent during all SL4 data taken.

It should be noted that the quartz on which the cap was mounted had two machined-in grooves which would have weakened it structurally. It may have been cracked by stresses induced during the launch or gimbal failure during SL3.

Therefore, a strong mechanical design in the feed structure is indicated for future sensors.

10.2.5 <u>Reference Loads</u>. Comparison of S193 and S194 Radiometer performance indicates that radiation-cooled reference loads for radiometers can be used in space instead of, or in addition to, a hot load to improve instrument calibration. Care must be taken to insure sufficient range and accuracy in the temperature sensors employed to monitor the reference loads.

10.2.6 <u>Progress in Microwave Technology</u>. Recently, considerable progress has been made in the manufacture of microwave semiconductor components and microwave integrated

circuits. This should mean improvement in the reliability of microwave sensors. Significant progress is being made in producing semiconductor devices with lower noise figures, higher gains and higher power outputs. Such devices will be able to replace vacuum tube and older semiconductor devices in many applications.

10.2.7 Progress in Computation Technology. Since the design of S193, minicomputer and microcomputer technology has developed rapidly. Today, a microcomputer could handle many of the functions performed in S193 by the Data Handling and Control Unit with lower space and power requirements. In fact, the rapid development of minicomputers and micro-computers makes onboard processing attractive for low and medium data acquisition rate systems. Future sensor devel-opment should seriously consider using onboard data proc-essing. Certain steps in this direction have already been taken in the airborne Passive Microwave Imaging System and the truck based Microwave Signature Acquisition System.

10.3 Data Handling And Processing
Conclusions And Recommendations

Experience with S193 indicates that it is of primary importance to begin consideration of data handling at the time of the specification and instrument design.

Close cooperation between design engineers, scientists, and computer programmers throughout the design, development, construction, and testing of the instrument will minimize problems encountered after scientific data collection begins. The data processing algorithms should be developed before

system testing begins and used in conjunction with raw system test data to finalize the algorithm and evaluate the system's performance.

The nature of microwave sensors, particularly passive sensors, is such that multipass (generally two-pass) data processing is necessary to obtain best results; since noise sources are required to calibrate radiometers, the calibration and baseline data is, by its very nature, noisy. To provide the test calibration, the noisy calibration data should be integrated for 5 to 25 times the length of the measurement time. To provide single calibration times, this length would be wasteful of observation time. Therefore, a number of short calibrations centered about the observation time should be averaged together in some manner. This could be done either by a "look ahead" capability in the data processing system, which requires keeping large volumes of data in core storage, or by using a more efficient two-pass data processing system.

One area which needs improvement is in the radiometer and scatterometer data display for oceanographers or other users. False color photos, computer contour maps, or other types of display should be explored to convey information to the users not familiar with the intricacies of microwave sensors.

10.4 Conclusions And Recommendations For Future Sensor Performance Evaluation

For future sensors, the evaluation of sensor performance should begin even before the sensor is purchased. A team of

professionals, including experts in sensor, target and atmosphere modeling, sensor hardware, data recording, processing, distribution and display requirements for probable applications, and the physics involved in these applications should be assembled to define and specify the new sensor. This team would utilize sensor simulation models for a proposed sensor similar to the ones developed for the S193 and "fly" them, using the computer, over target and atmosphere models such as those developed by Paris to produce simulated data. This simulated data would be processed and analyzed to aid in determining the required sensor performance levels for each application. The required sensor performance levels plus a safety margin to cover degradation in an operational environment would be used to specify the system.

The sensor hardware and software experts would monitor and assist in the development and construction of the sensor, while other members of the team assisted in specifying the testing required for accurate sensor characterization for modeling, calibration, and data reduction.

Data handling and processing algorithms should be developed in parallel with system construction and be available during system acceptance testing.

Experience with S193 indicates that careful test site selection with adequate ground truth is essential to a successful evaluation of sensor performance.

S193 experience also indicates that the sensor performance evaluation team should have priority in receiving

raw and processed data from the sensor. This will enable
production data processing and distribution facilities to
proceed with confidence and efficiency after the sensor
performance evaluation group has completed data evaluation.

10.5 Accomplishments Associated with S193[22]

The Skylab S193 Radiometer/Scatterometer/Altimeter
experiment was man's first attempt to gather data using
earth-oriented, spaceborne, active microwave systems. For
the first time, nearly simultaneous radiometric brightness
temperature and radar backscatter data were acquired over
land and ocean scenes using a spaceborne microwave sensor.

The S193 receiver and processors were designed to
measure powers from 10^{-15} watts to 10^{-10} watts while sur-
viving in an environment with peak transmitted powers of
2,000 watts. This represents an advancement in microwave
remote sensing technology. The definition of sensor speci-
fications, mission requirements, data handling, and ground
truth coordination for the NASA GEOS-C and SEASAT-A programs
was directly influenced by the performance and data analysis
of the S193 sensor.

The ocean panel of a NASA-organized Active Microwave
Workshop, outlining applications and systems for future
aerospace programs, used inputs from the S193 data analysis
along with other data to recommend, design and develop higher
precision scatterometer, altimeter; and radiometer for future
remote sensing programs.

During the last portion of the Skylab-3 mission, the
antenna gimbal malfunctioned. The recommended fix procedure
was to disable the pitch gimbal electrically and pin the
antenna in the pitch axis. Astronauts completed the fix in
space, demonstrating that complex electronic systems can be
repaired to extend their operating life in space. Techniques
for the repair of electronic systems in space can be effi-
ciently employed in the Space Shuttle program where the
electronic systems are expected to operate over extended periods.

The S193 system gathered data in a large number of
intrack and crosstrack modes over land and ocean surfaces.
In addition, data was also gathered looking at deep space,
for sensor performance evaluation, and for revision to the
preflight calibrations. While Skylab-2 was in progress, Ava,
the first Pacific hurricane of the season was forming. A
pass was completed over Ava on June 6, 1973 and data was
gathered in the crosstrack non-contiguous mode. A comprehen-
sive remote sensing study of hurricane Ava was accomplished
by the joint efforts of NASA and the National Oceanic and
Atmospheric Administration (NOAA) encompassing aircraft,
satellite, and Skylab observations with a number of micro-
wave sensors. This was a first in the remote sensing study
of a hurricane.

The evaluation of the S193's inflight performance was
highlighted by the deployment and operation of an array of
ground-based microwave receivers to measure the antenna pat-
tern and scan performance, scatterometer-transmitted power,
pulse rate, and duration. The primary purpose of this study
by the University of Kansas was to measure changes in antenna
performance which might have resulted from the launch and

space environments. The altimeter pulse shape, duration, spacing, and amplitude were recorded by the NASA Wallops Space Center. The results of the S193 sensor performance evaluation have been used in revising the data processing to reflect the actual inflight performance of the sensor. More important, a methodology has been developed for the inflight evaluation of future spaceborne microwave sensors.

The progress made in the development of microwave technology toward more sophisticated future spaceborne earth-oriented microwave sensors, the investigations of earth phenomena, and the procedures for future missions resulting from the S193 program should be supplemented with the lessons of experience. This experience and progress should represent a significant step toward the ultimate goal of using, operationally, the spaceborne microwave sensors for sensing earth resources phenomena. Future microwave programs demand development of high precision side-looking, imaging radars in addition to scatterometers, altimeters, and radiometers with multiple frequency, multiple polarization, and better antenna designs to achieve this goal.

11.0 REFERENCES

1. Krishen, K.; and Pounds, D.: S193 Radiometer and Scatterometer Sensor Mathematical Models. LEC 1741, Lockheed Electronics Company, Inc., Houston, Texas, February 1974.

2. Paris, Jack F.: Marine Radiometry and its Application to Marine Meteorology and Oceanography. Department of Meteorology, Texas A&M University, College Station, Texas, January 1969.

3. Paris, Jack F.: Transfer of Thermal Microwaves in the Atmosphere. Volume I, Department of Meteorology, Texas A&M University, College Station, Texas, May 1971.

4. Paris, Jack F.: Prediction of the Response of Earth Pointed Sensors (PREPS), Passive Microwave Sensors Report. LEC/HASD 640-TR-105, Lockheed Electronics Company, Inc., Houston, Texas, March 1972.

5. Welch, W. J.: Reachie, S.; Thornton, D.D.; and Wrixon, G.: "Measurement of the Cosmic Background at 1.5 cm Wavelength," Physical Review Letters, Volume 18, Number 24, June 12, 1967, pp. 1068-1070.

6. Webster, Adrian. "The Cosmic Background Radiation", Scientific American, August 1974.

7. Hall, Forrest G.: "Microwave Brightness Temperature of a Windblown Sea", Fourth Annual Earth Resources Program Review, NASA Manned Spacecraft Center, Volume I; January 1972.

8. Stogryn, A.: The Apparent Temperature of the Sea at Microwave Frequencies. IEEE Trans. Ant. and Prop., Vol. AP-15, March 1967, pp. 278-286.

9. Wagner, R. J. and Lynch, P. J.: Analytical Study of Microwave Sea Brightness Temperatures: A Composite Surface Model. Final Report, TRW Systems Group, Redondo Beach, California, Contract N00014-71-C-0240, December 1972..

10. Hollinger, J. P.: "Mission 119 Passive Microwave Results" Fourth Annual Earth Resources Program Review, Vol. IV, NASA Manned Spacecraft Center, January 1972.

11. Hall, Forrest G.: Private Communications

12. Mendlowitz, Maury: Interim Report; Mesiah Program. LEC/HASD 640-TR-168, Lockheed Electronics Company, Inc., Houston, Texas, April 1973.

13. Philco Ford Corporation: "TR 524 Earth Resources Production Processing Requirements for EREP Electronic Sensors." Section 6, April 1975, Revision B.

14. Dixon, Wilfrid J. and Massey, Frank J., Jr.: Introduction to Statistical Analysis. 2nd Ed., McGraw-Hill, 1957, pp. 76, 405.

15. Carney, J. J.: Skylab S194 Microwave Radiometer Sensor Performance Evaluation: Final Report, LEC-5862, Lockheed Electronics Company, Inc., Houston, Texas, April 1975.

16. Eisenhart, Churchill, "Expression of the Uncertainties of Final Results." Science, Vol. 160, June 14, 1968, pp. 1201-1204.

17. Ku, Harry H.: "Expression of Imprecision, Systematic Error and Uncertainty Associated with a Reported Value," Measurements and Data July - August 1968, pp. 72-77.

18. Tiuri, Martti E., "Radio Telescope Receivers." Radio Astronomy by John D. Kraus, McGraw-Hill, New York, 1966.

19. Murphy, R. B.: "On the Meaning of Precision of Accuracy." Materials, Research, and Standards, American Society Testing Materials, April 1961, pp. 264-267.

20. Private Communications from Arun Sobti and A. C. Cook.

21. Private Communications from R. Eisenberg.

22. Krishen, Kumar.: The Significance of the S193 Skylab Experiment Using Preliminary Data Evaluation. LEC-4250, Lockheed Electronics Company, Inc., Aerospace Systems Division, March 1975.